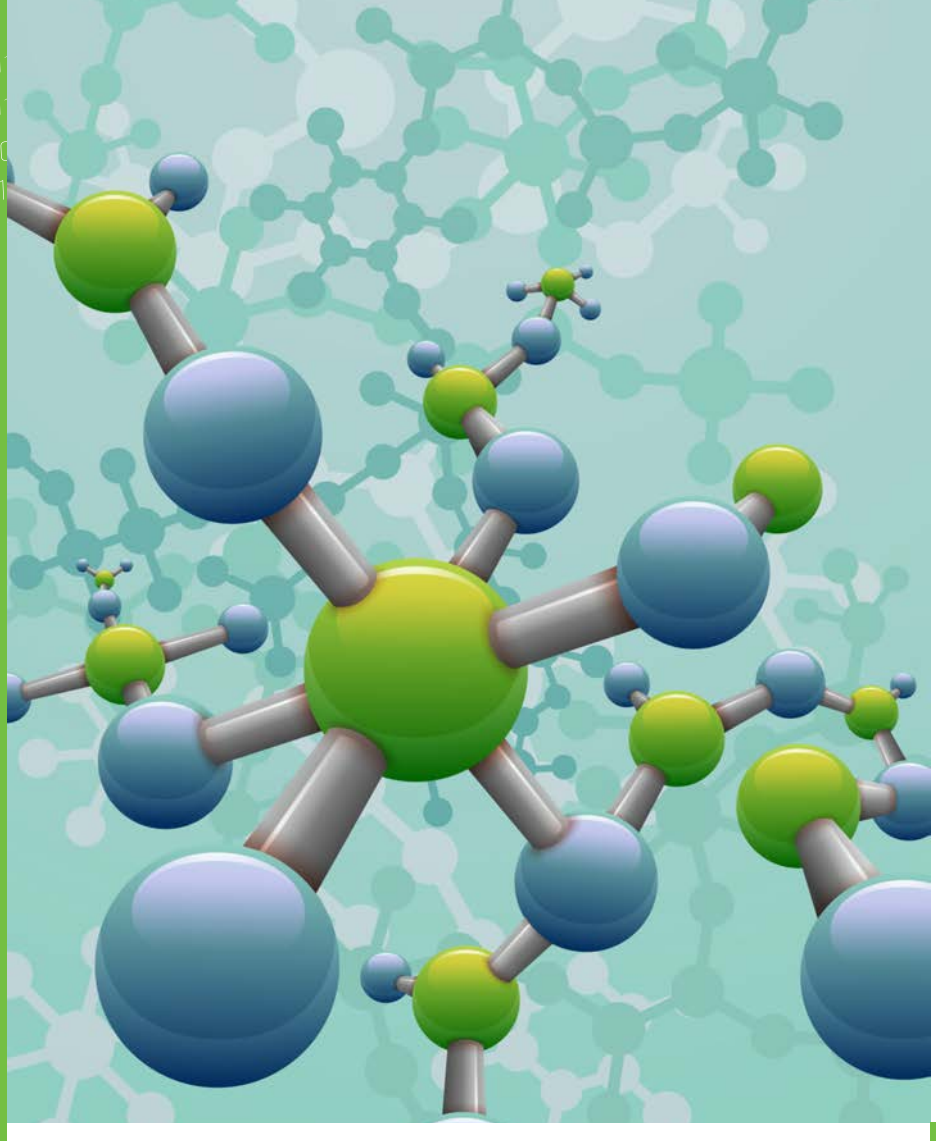

SCIENCE • TECHNOLOGY • RESEARCH HIGHLIGHTS • VISIONS •

Dissertation
97

Improving sealing, electrical contacts, and corrosion resistance in solid oxide fuel cell stacks

Markus Rautanen

VTT

VTT SCIENCE 97

Improving sealing, electrical contacts, and corrosion resistance in solid oxide fuel cell stacks

Markus Rautanen

Thesis for the degree of Doctor of Science to be presented with due permission of the Aalto University School of Science for public examination and criticism in Auditorium K216, at Aalto University (Espoo, Finland), on the 8th of June, 2015 at 12 noon.

ISBN 978-951-38-8313-3 (Soft back ed.)
ISBN 978-951-38-8314-0 (URL: http://www.vtt.fi/publications/index.jsp)

VTT Science 97

ISSN-L 2242-119X
ISSN 2242-119X (Print)
ISSN 2242-1203 (Online)

JULKAISIJA – UTGIVARE – PUBLISHER

Teknologian tutkimuskeskus VTT Oy
PL 1000 (Tekniikantie 4 A, Espoo)
02044 VTT
Puh. 020 722 111, faksi 020 722 7001

Teknologiska forskningscentralen VTT Ab
PB 1000 (Teknikvägen 4 A, Esbo)
FI-02044 VTT
Tfn +358 20 722 111, telefax +358 20 722 7001

VTT Technical Research Centre of Finland Ltd
P.O. Box 1000 (Tekniikantie 4 A, Espoo)
FI-02044 VTT, Finland
Tel. +358 20 722 111, fax +358 20 722 7001

Juvenes Print, Tampere 2015

Preface

The work presented in this thesis has been carried out in VTT Technical Research Centre of Finland between 2008 and 2014. Financial support from VTT Technical Research Centre of Finland, the Fuel Cells and Hydrogen Joint Undertaking and TEKES – the Finnish Funding agency for Innovation is acknowledged.

The work presented in this thesis has been completed with the help of many persons. I would like to thank my instructors Jari Kiviaho and Olli Himanen for encouraging me in starting doctoral studies in the first place and for the support that I have received over the years. I would also like to thank Peter Lund for accepting me as a student in the department of applied physics and being very flexible with my studies. I want to thank the whole fuel cell team at VTT, especially Jari Kiviaho, Olli Himanen, Olivier Thomann, Kari Koskela, Johan Tallgren and Valtteri Pulkkinen for close collaboration and for the relaxed atmosphere.

For my parents, Marja-Leena and Pentti: thank you for always encouraging me to study while never pushing me towards any particular profession or career. Certainly the most efficient person in taking my mind of work has been my son Otso – thank you for that. The most grateful I am to my wife Tanja. With you I have had the privilege to share many of the best moments in my life. Hopefully there is still many more awaiting behind the horizon.

Espoo, 14.5.2015
Markus Rautanen

Academic dissertation

Supervising professor

Professor, Dr. Peter Lund
Department of Applied Physics
Aalto University School of Science
Espoo, Finland

Thesis advisors

Dr. Jari Kiviaho
Chief Research Scientist
Fuel Cells
VTT Technical Research Centre of Finland Ltd
Espoo, Finland

D.Sc. Olli Himanen
Senior Research Scientist
Fuel Cells
VTT Technical Research Centre of Finland Ltd
Espoo, Finland

Reviewers

Dr. Tero Hottinen
General Manager
Business Innovation
Wärtsilä
Helsinki, Finland

Dr. Bin Zhu
Assosiate Professor
Advanced fuel cell and solar cell group
Royal Institute of Technology (KTH)
Stockholm, Sweden

Opponent

Professor, PhD Alan Atkinson
Department of Materials
Imperial College
London, United Kingdom

List of publications

This thesis is based on the following original publications, which are referred to in the text as I–VI. The publications are reproduced with kind permission from the publishers.

I. **Rautanen, Markus**; Himanen, Olli; Saarinen, Ville; Kiviaho, Jari
Compression properties and leakage tests of mica-based seals for SOFC stacks
Fuel Cells. Vol. 9 (2009) No: 5, 753–759

II. **Rautanen, Markus**; Pulkkinen, Valtteri; Tallgren, Johan; Himanen, Olli; Kiviaho, Jari
Effects of the first heat up procedure on mechanical properties of solid oxide fuel cell sealing materials
Journal of Power Sources. Elsevier. Vol. 284 (2015), 511–516

III. Hoyes, John; **Rautanen, Markus**
SOFC sealing with Thermiculite 866 and Thermiculite 866 LS
ECS Transactions. Electrochemical Society. Vol. 57 (2013) No: 1, 2365–2374

IV. **Rautanen, Markus**; Thomann, Olivier; Himanen, Olli; Tallgren, Johan; Kiviaho, Jari
Glass coated compressible solid oxide fuel cell seals
Journal of Power Sources. Elsevier. Vol. 247 (2014), 243–248

V. Thomann, Olivier; Pihlatie, Mikko; **Rautanen, Markus**; Himanen, Olli; Lagerbom, Juha; Mäkinen, Maija; Varis, Tommi; Suhonen, Tomi; Kiviaho, Jari
Development and application of HVOF sprayed spinel protective coating for SOFC interconnects
Journal of Thermal Spray Technology. ASM; Springer. Vol. 22 (2013) No: 5, 631–639

VI. Thomann, Olivier; **Rautanen, Markus**; Himanen, Olli; Tallgren, Johan; Kiviaho, Jari
Post-experimental analysis of a SOFC stack using hybrid seals
Journal of Power Sources. Elsevier. Vol 274 (2015), 1009–1015

Author’s contributions

For Publications I and IV, the author had primary responsibility for all parts of the publication.

For Publication II, the author had primary responsibility for the design of experiments, interpretation of results, and writing.

For Publication III, the author conducted part of the measurements and actively participated in the writing process.

For Publications V and VI, the author actively participated in analysis of the results and in the writing process.

Contents

List of symbols

A	Anode
AFC	Alkaline fuel cell
ASR	Area specific resistivity
BSE	Back scattered electron imaging
c	Concentration
C	Cathode
CEV	Chemically exfoliated vermiculite
cross	Cross leak between anode and cathode
D	Diffusion coefficient
EDS	Energy dispersive spectroscopy
F	Faraday constant
ΔG	Change in Gibbs free energy
H_2	Hydrogen molecule
H_2O	Water/steam molecule
HVOF	High velocity oxygen flame
I	Electrical current
J	Diffusion flux
LSCF	Lanthanum strontium cobalt ferrite, $La_xSr_{1-x}Co_yFe_{1-y}O_{3-\delta}$
LSM	Lanthanum strontium manganite, $La_{1-x}Sr_xMnO_3$
NASA	National Aeronautics and Space Administration
NTP	Normal temperature and pressure (273.15 K, 1013.25 mbar)
OCV	Open circuit voltage

p	Pressure
$\dot{Q}$	Flow
R	Gas constant
t	Time
T	Temperature
PAFC	Phosphoric acid fuel cell
PEMFC	Proton electrolyte membrane fuel cell
SEM	Scanning electron microscopy
SOFC	Solid oxide fuel cell
TEC	Thermal expansion coefficient
TOT	Total
V	Volume
X	Fraction
YSZ	Ytria stabilized zirconia

1. Introduction

1.1 Background

Today's world is dominated by fossil fuel-based energy production. It is at the moment under debate when exactly these non-renewable sources of energy will run out, but it is very clear that sooner or later an energy system based on renewable energy sources needs to be established. Before the balance of energy production shifts to renewable energy sources, energy production efficiency should be of high concern, to make sure that both renewable and non-renewable energy is utilized with the highest possible efficiency. Fuel cells can contribute to energy production during and after this change: they can directly convert chemical energy of fuel and oxidant to electricity with high efficiency and low emissions. Fuel cells can operate with a variety of fuels such as natural gas, biogas or hydrogen.

The fuel cell is an invention first mentioned in 1839 by German physicist William Schönbein in The London and Edinburgh Philosophical Magazine and Journal of Science [1]. However, it took more than a century for the technology to reach sufficient maturity for the first significant applications to emerge. Since the 1950s, fuel cells have played a part in, for example, NASA's space flight programmes, producing electricity and water during space missions [2]. Development of fuel cell-powered vehicles started in the early 1990s, and several manufacturers have now completed field trials, and market entry is expected during 2015 [3]. In the field of stationary power production, fuel cells are also gaining more ground and installations of fuel cell power plants have exceeded 180 MW with a fast growth rate of about 50 MW of new installations in 2013 [4].

Fuel cells are commonly divided into different groups based on their operating temperature and electrolyte. Low-temperature fuel cells such as the polymer electrolyte fuel cell (PEMFC) and alkaline electrolyte fuel cell (AFC) are used in automotive and mobile applications. High-temperature fuel cells such as the phosphoric acid fuel cell (PAFC) and solid oxide fuel cell (SOFC) are used mostly in stationary heat and power generation, mostly due to their ability to utilize hydrocarbon fuels such as natural gas. The work presented in this thesis is focused on the solid oxide fuel cell.

Current challenges of SOFCs can be easily summarized: insufficient lifetime and high capital costs. At the moment, capital expenditure on a stationary SOFC system such as a 100 kW system offered by Bloom energy Ltd is in the order of $7000/kW, and the cost of residential CHP systems in the range of 1…10 kW is around $25000/kW [5]. This figure needs to be reduced to around $1000/kW to allow entry to non-subsidized markets [6]. At the same time, the high operating temperature of SOFCs creates challenges for the materials, causing performance degradation over the operating time. Currently, state-of-the-art SOFC stacks have a lifetime of around 5000…10000 h, which needs to be expanded to the range of 20000…40000 h [7]. The heart of any SOFC power system is a stack in which the electrochemical reactions take place. Stack cost is estimated to be around 40…60% of the total system cost [8]. Therefore, this is the area where most of the performance gains and cost reduction needs to take place.

1.2 Objectives of this thesis

The goal of the work presented in this thesis was to achieve performance and lifetime enhancement in SOFC stacks. Four major targets were set for this work:

1. A SOFC stack sealing material capable of 20% compression using maximum of 1 MPa compressive stress
2. Sealing material capable of maintaining leak levels below 1% of inlet fuel flow using a maximum of 1 MPa compression
3. A decrease in-stack electrical contact losses below 1% at 0.3 Acm^{-2} current density
4. A target stack lifetime of 10 000 h with reduction of chromium evaporation from interconnect steels and no significant corrosion between other stack materials.

The compression of the sealing materials affects stack design and manufacturing of other components around the seal. For example, if the sealing material's ability to compensate for manufacturing variation of other components is high, this increases the manufacturing yield of other components, as their dimensional tolerances can be wider. This naturally has a direct influence on the manufacturing costs of the whole stack. For example, the anode support of the SOFC cell manufactured via tape casting route has a thickness variation of the order of 1…5% [9,10]. To be sure that cell-to-cell thickness variation within a stack does not significantly affect the apparent stress on the seal and therefore gas tightness, the compressibility of the seals needs to be significantly higher than the cell-to-cell thickness variation. As shown in chapter three of this work, compressibility of conventional compressible sealing materials such as mica papers is only in the order of 3% per megapascal of applied stress. This calls for stress levels of at least several megapascals, which are impractical as material thicknesses should

be reduced to gain cost savings. Therefore a target of 20% compression at 1 MPa was set for the sealing development work.

Any loss of electrical power capability inside the fuel cell stack is away from the actual net power production of the whole system. The second goal of this work is related to decreasing in-stack leakage which directly influences the electrical efficiency of the cell, as less fuel is wasted in leakage-induced burning. Therefore an overall target for the sealing material to be developed was a leak rate of less than 1% of inlet fuel with 1 MPa of compression and 20% of compressibility.

The third goal also focuses on improving the electrical efficiency of the stack by decreasing resistive losses inside the stack. These can occur, for example, by contact losses or corrosion-related growth of insulating oxide layers. Diminishing these contact losses below 1%, at a typical 0.3 Acm^{-2} current density of SOFC stacks, would have a beneficial effect on the electrical efficiency of the stack. The fourth goal targets an enhanced stack lifetime. If the lifetime can be improved, this will also have a beneficial impact on cost, as stack changes in a system will become less frequent. In total, these performance and lifetime improvements will lower the cost per produced energy unit of SOFC technology, making it more competitive in the energy markets.

This thesis starts with a short introduction to the field in chapter two. Chapters 3–5 summarize Publications I–VI. Chapter 6 presents the conclusions of the work and the outlook for future research in the field.

2. SOFC stack technology

2.1 Basics of solid oxide fuel cell stacks

A fuel cell is a device that converts the chemical energy of fuel and oxidant directly into electricity and heat. This is achieved by the electrochemically active cell, which can operate at electrical efficiency in excess of 60%. A solid oxide fuel cell consists of three main components: a dense electrolyte and anode and cathode electrodes. Figure 1 shows the basic operating principle of a SOFC cell. Oxygen (air) is fed into the cathode and oxygen ions move through the electrolyte to the anode, reacting there with fuel. Electrons move through the outside circuit from anode to cathode. Typical layouts are anode supported and electrolyte supported cells. In an anode supported structure, the anode layer is usually 100…500 µm thick and used as a substrate, over which thin electrolyte and cathode layers are constructed by, for example, screen printing. In an electrolyte supported structure, the electrolyte is relatively thick (100…200 µm) and used as a mechanical support, over which the porous electrodes are constructed.

SOFC electrolyte materials, such as zirconia doped with yttria, require operating temperatures in excess of 500 °C to reach sufficient ionic conductivity. Typical, modern SOFC stacks operate at temperatures of 600…850 °C. This is seen as an optimum operating area where sufficient cell-level performance is achieved, internal reforming of methane is still possible [11], while the relatively low operating temperature allows the use of ferritic stainless steels as interconnects. Table 1 presents a few SOFC cell manufacturers and the main characteristics of their cells.

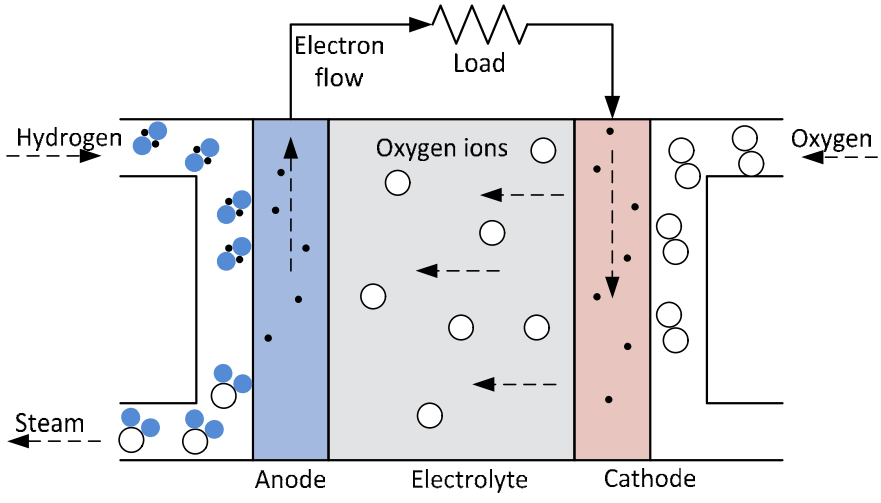

Figure 1. Principle of solid oxide fuel cell.

Table 1. Common manufacturers of SOFC cells.

Manufacturer	Mechanical support	Typical operating temperature / °C	Typical cell size / cm^2	Reference
Elcogen AS	Anode	600…800	100	[10]
SOFCMAN	Anode	700…800	100	[12]
SOFCMAN	Electrolyte	850	100	[12]
Kerafol/HCStarck	Electrolyte	750…950	100	[13]
Versa Power Systems	Anode	650…800	550	[14]

The power of a single cell is often insufficient, so a number of cells are incorporated into a stack assembly. Other main components of a typical SOFC stack are interconnects and seals, which are used to direct gas flows and electricity through the stack [15]. There are two main fields of SOFC stacks: planar and tubular designs. Typical advantages associated with tubular design are rapid start-up times and ease of sealing, whereas a planar design holds more promise for cheaper mass manufacturing costs and higher power density [15]. The focus of this thesis is on the planar type of fuel cell stacks with metallic interconnect plates.

Stack designs vary considerably from one manufacturer to another, but commonly the cell is located roughly in the centre of the interconnect, and inlet and outlet gas streams flow at the perimeter of the interconnect in separate manifolds. The cell and manifolds are sealed to prevent anode and cathode gases from mixing with each other. Figure 2 shows an example of an SOFC stack construction. Cells, interconnects, and seals of different geometries are stacked into a tower-like structure to increase the total power. At both ends of the stack are endplates that seal the manifolds from the surroundings and provide means to connect the stack to fuel and air pipelines. Electrical current is either collected from the endplates or from specific current collector plates near both ends of the stack.

Stacks are often described according to their flow configuration, meaning the direction of anode and cathode flows over the cell. The usual flow configurations are cross-flow, co-flow, and counter-flow [16]. There are also more complicated flow geometries or mixtures of the previous three basic types (see e.g. [17]).

While still a few years ago, stacks were mostly based on cells of around 100 cm^2 with a total power range around 1 kW, currently there are several stack designs based on larger cell areas offering electrical power in the range of 5…10 kW [18,19].

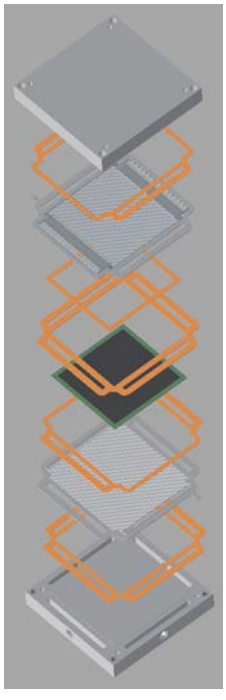

Figure 2. Typical SOFC stack construction (only a single repetitive unit shown for clarity).

2.2 Interconnects

Interconnect plates need to provide good electrical connection from cell to cell and separate anode and cathode atmospheres. It is also beneficial if the interconnects can offer mechanical support to the stack structure. In the SOFC stack, heat is generated in the cells, and therefore it is also beneficial if the heat conduction capability of interconnects is high so that they can help in transferring heat from the cell.

In the early stage of SOFC technology, interconnects were often made of ceramics such as $LaCrO_3$ based materials. The downsides of $LaCrO_3$ materials include their low electrical conductivity at temperatures below 800 °C and relatively expensive manufacturing [20]. Lanthanum chromites also exhibit swelling in reducing atmospheres leading to internal stresses and possibly cracking (see e.g. [21] for more details). Advancements made in the cell technology have made it possible to lower the operating temperature from 900…1100 °C of early SOFC cells to the 600…900 °C range. This allows relatively cheap metallic interconnects to be used.

A typical interconnect plate has gas channels against the cell to provide space for the reactants to flow along the cell and enough contact area for a good electrical conductivity. Figure 3 shows an example of an SOFC interconnect. The ribs and valleys in the middle of the plate form contact areas against the cell and gas channels respectively. At the perimeter of the interconnect are gas manifolds for air and fuel.

The main drivers in using ferritic stainless steels are ease of manufacturing, price, and the thermal expansion coefficient (TEC), which closely matches that of the SOFC cell [22]. Metallic interconnects are usually manufactured of ferritic high-temperature steel. The most common steel grades used as interconnects are Crofer 22 H [23], AISI 441 [24], ZMG232L [25], Sanergy HT [26], E-Brite [27], and CFY [28].

Table 2 contains the main elements present in these materials. The five first materials are all ferritic stainless steels, with AISI 441 having the lowest chromium content of 18% compared to 26% of E-Brite. The last material (CFY) is a chromium-based alloy manufactured through a powder metallurgical route. The high chromium content and low aluminium and silicon content of these alloys results in the formation of chromium rich oxide scales. This is beneficial as the conductivity of chromium oxide is in the range of 0.1…1 Ωm, which is about 10^5 times higher compared to alumina [29].

Metallic interconnects can be manufactured from bare steel by, for example, machining, punching, coining, hydro-forming, or laser-cutting methods. Typically in the case of thin (<1 mm) interconnects, forming techniques such as stamping or hydroforming are common, while thicker interconnects are often machined into shape. As the cost of the material is directly related to its weight, thin interconnects are of primary interest. However, decreasing material thickness usually has

an effect on the durability as well, so this needs to be balanced with cost-saving potential. For example, Huczkowski et al. have observed that doubling the thickness of uncoated Crofer 22 APU or ZMG232 steels roughly doubles their lifetimes [30].

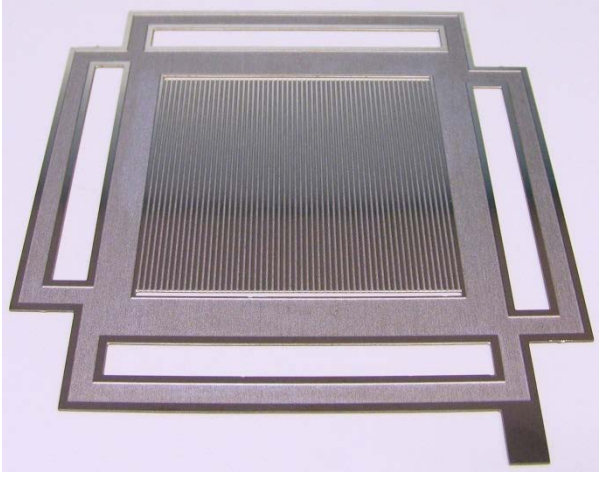

Figure 3. Interconnect.

Table 2. Chemical compositions of typical metallic interconnect materials in mass percentages.

Material	Fe	Cr	Ni	C	Si	W	Nb	Ti	Y	Al	Mn
Crofer 22 H	bal	22		0.015	0.3	1.5	0.6	0.01			0.6
AISI 441	bal	18		0.02	<1		0.3	0.3			
ZMG232L	bal	22	<0.7	<0.1	<0.1						
Sanergy HT	bal	21.2		0.040	<0.3		0.71			0.017	
E-Brite	bal	26	0.15	0.002	0.20						0.05
CFY	5	bal		<0.025	<0.12				0.1	<0.12	

2.3 Interconnect coatings

In SOFC stacks, interconnects are subjected to a reducing atmosphere on one side and an oxidizing atmosphere on the other side. This, together with a cost-driven need to use thinner interconnects, creates severe material challenges. Corrosion of interconnects can lead to mechanical failure of the stack, poisoning of the cell by volatile species, an increase of contact resistance between cell and interconnect, or short-circuiting over one or more cells. A number of coating methods have been developed to mitigate these corrosion effects.

One of the most significant reasons for the cell performance degradation is chromium poisoning. This happens when the chromium oxide scale of the metallic interconnect is subjected to humidity and oxygen. In the presence of humidity, chromium oxyhydroxide is the dominant species [31,32] and formed according to equation (1) [33].

$$Cr_2O_3(s) + 2H_2O(g) + 3/2O_2(g) \rightarrow 2CrO_2(OH)_2(g) \qquad (1)$$

The gaseous chromium oxyhydroxide can reduce at the cathode, and the chromium deposited there causes loss of electrochemical performance [34]. To minimize the effect of cell performance degradation due to chromium poisoning, metallic interconnects are usually coated with either perovskites [35,36,37], spinels [38] [39], or metals [26]. The purpose of these coatings is to form a barrier layer that inhibits chromium evaporation from the interconnect steels.

Common methods of application of chromium barrier coatings are wet powder spraying [15], thermal spraying [40,41,42], chemical vapour deposition processes [43,44] such as atomic layer deposition [45], and physical vapour deposition processes [26]. Coating is usually carried out by the stack manufacturer, although, for example, Sandvik offers steels such as Sanergy HT already pre-coated with cobalt or ceria and cobalt [26].

2.4 Stack sealing

An ideal SOFC stack-sealing material should be gas tight and have good compressibility and conformability. It should naturally also be resistant to SOFC operating temperatures and be chemically stable with gas atmospheres, as well as with neighbouring components. Sealing that is placed between different electrical potentials within a stack also needs to be electrically insulating. The requirement of gas tightness is quite severe, as any leak will directly decrease the electrical efficiency of the stack and also cause a local hot spot that could induce material

degradation. Localized leak also increases the local fuel and/or air utilization which can lead to e.g. oxidation of the anode.

Stack seal should also function as a spacer between adjacent components. It is often the case that the seals are practically the only flexible components in a stack, so they need to be able to take up any manufacturing or assembly-related tolerances.

Traditionally, SOFC stacks have been sealed with glass- and glass-ceramic materials (see e.g. [46,47,48]). Glass-based seals bond to the adjacent surfaces and can offer very gas tight sealing if properly designed, heat-treated, and operated. The downsides can include a need for a well-controlled joining procedure during the first heat up [49], cracking under mechanical stress, chemical reactions at interfaces to be joined, and brittleness at low temperatures. As an example, Figure 4 shows a SEM cross section of a typical glass-ceramic material, H.C. Starck HSC3 after 100 h at 700 °C. Two different phases and black pores can be identified from the micrograph. A lot of work has concentrated on manufacturing glass-based sealing materials that have a similar coefficient of thermal expansion compared to SOFC cells. For more details, see [50,51,52,53,54].

Another group of sealing materials is compressible seals. Stacks with compressible seals can usually be easily assembled, and they require no special joining procedure. Traditionally, materials from a group called mica have been used to seal SOFC stacks. Mica is a group of silicate minerals with a general structure of $AB_{2\text{-}3}(Al,Si)\text{-}Si_3O_{10}(OH)_2$ in which A is either K, Na, Ca, or Ba, and B is either Al, Fe, Mg, or Li [55]. Micas can also contain other elements such as F^- replacing some of the OH^- ions [56]. Of this group, phlogopite ($KMg_3(AlSi_3O_{10})(OH)_2$) mica is by far the most common. Phlogopite mica papers are being sold under different brands, such as Statotherm HT by Burgmann Industries [57] and Cogemica by Cogebi. Figure 5 shows the cross sectional SEM-image of Statotherm HT. Vertical, interleaving phlogopite platelets are clearly seen in the image. The drawback of these types of compressible materials is the requirement of compressive stress in excess of several MPa to form a gas tight seal. Their leak rates are usually higher compared to bonding seals and the leak rates are dominated by the interfacial leak paths, especially at low compressive stresses [58,59,60,61,62].

Flexitallic Ltd. has developed a series of materials under a trade name Thermiculite, which are claimed to lower compressive stress requirements. Thermiculite 866 and Thermiculite CL87 consist of only chemically exfoliated vermiculite and steatite, also known as talc; there is no other component and no organic binder. The sheets of the CEV act as a binder to hold the whole together to form a flexible sheet that is robust enough to be cut into complex shapes [63,64]. Figure 6 shows the cross-section of Thermiculite 866. Horizontal vermiculite platelets (light grey) are seen between steatite filled areas (dark grey).

In recent years, some attention has been generated by a solution known as hybrid seals. These seals have a compressible core with conformable layers on both sides of the core to provide enhanced sealing at the interfaces. The interfacial

layers are usually made of glass or metal foil. These materials are targeted to be used under low (<2 MPa) compressive stresses while maintaining the easy handling and assembly associated with compressible seals (see e.g. [65,66] for more details).

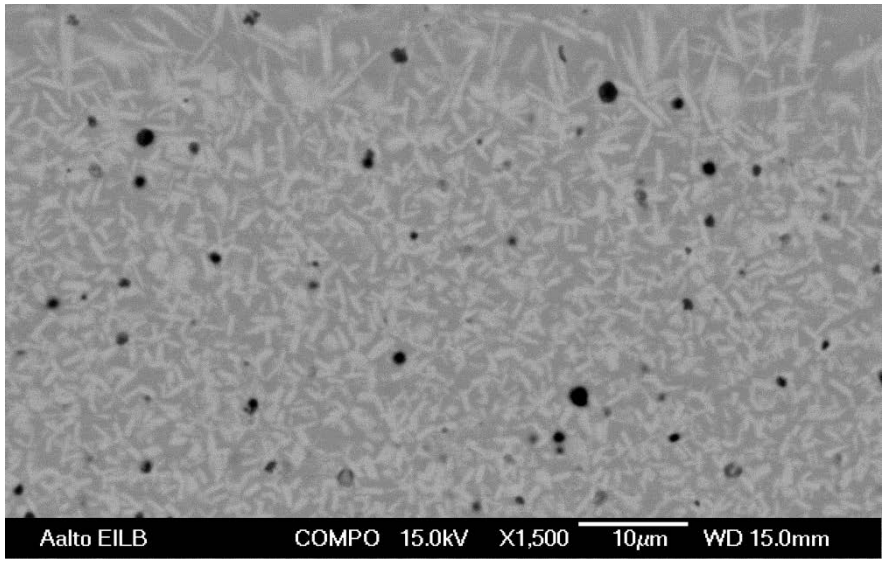

Figure 4. SEM image of H.C. Starck Ampergy HSC3 glass-ceramic sealing material.

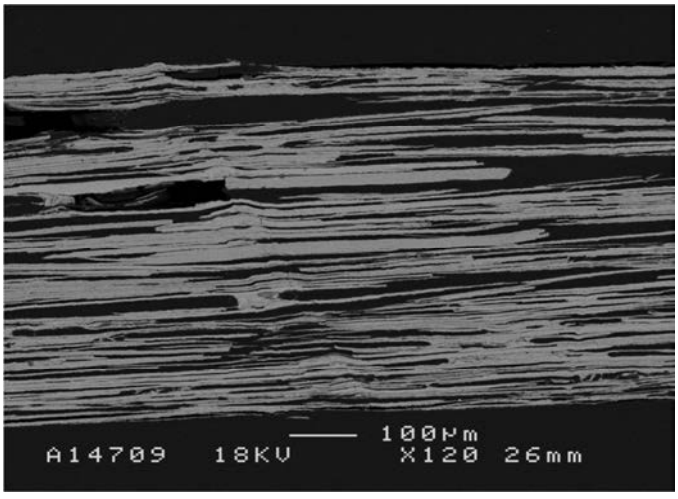

Figure 5. SEM image of Statotherm HT (phlogopite mica paper).

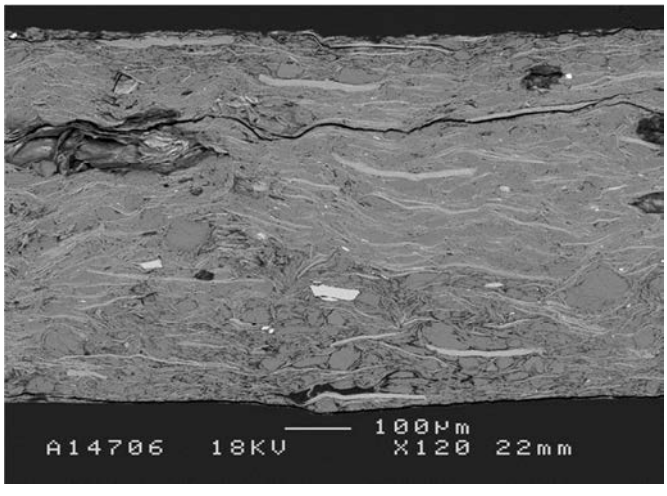

Figure 6. Cross-sectional SEM image of Thermiculite 866.

3. Mechanical properties of SOFC sealing materials

3.1 Background

The primary function of SOFC stack seals is the ability to effectively separate cathode and anode gases from each other and from the surroundings. As the seal is often the only non-rigid component within a stack, it needs to take up the manufacturing and assembly tolerances of other components. To this end, the sealing material needs to have a sufficient amount of compressibility. Figure 7 displays a simplified sealing arrangement of a typical SOFC stack. In a perfectly engineered sealing solution, the seal provides a gas-tight barrier between adjacent components (a). If the seals are too thick, the gas tightness of the stack might be good, but this would often result in poor electrical contact between interconnects and cells, as the compressive stress is mostly on the seals and not on the cell (b). On the other hand, if the seals are too thin, electrical contact might be good but the gas tightness is poor, at least in the case of compressible seals, due to the cell carrying most of the compressive stress (c). In the last two cases, mechanical stresses on interconnects are usually also higher due to uneven stress distribution. Therefore, an optimal sealing solution needs to balance between achieving low contact resistance between cell and interconnect, and gas tightness to obtain maximum stack performance.

The progress in manufacturing SOFC cells is leading to an increase in cell area. Increasing the cell size is intriguing for the stack manufacturer, as the number of components needed in a stack is decreased for the same amount of power. From the perspective of compressible seals, the increase in cell area presents a challenge: the higher the cell area, the higher the required compressive force for the stack. Increasing the external forces to the stack includes a risk of either deforming or breaking stack components should the forces not be optimally distributed. Higher external forces will also result in more bulky components both inside the stack and in the stack compression mechanism. The mechanical compression of a stack is often needed at a lower temperature than the operating temperature,

as, for example, steel springs cannot be relied upon at SOFC operating temperatures, leading to heat loss from the stack along the compression rods or structures.

Typically, SOFC stacks are assembled at room temperature, then heated up and conditioned, and then operated at temperatures in the range of 600…900 °C. This creates a need to understand the mechanical properties of the seals not only at room temperature or at operating temperature, but throughout the whole operating region. Of special interest are the mechanical properties of materials during the first heat up, in which the stack is sealed, reduced, and tested.

In publications I-III, the mechanical properties of SOFC sealing materials were studied. Compressibilities of the materials were analysed as a function of temperature. Especially the mechanical behaviour of compressible sealing materials, as well as a glass material, was studied during the first heat-up procedure.

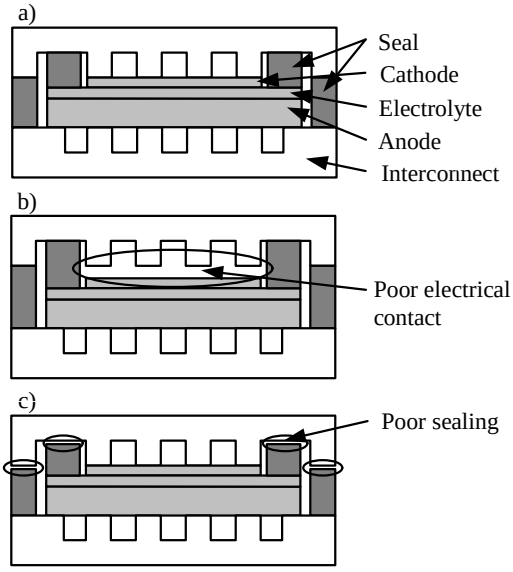

Figure 7. Stack sealing challenges with different seal thicknesses. Low contact-stress areas have been indicated with circles.

3.2 Experimental

Mechanical properties of sealing materials were evaluated as a function of compressive stress and temperature. Figure 8 shows a schematic of the equipment used in the low compressive stress (<1 MPa) measurements. A sample is inserted between the measurement rods, and a weight is clamped on the top of both rods. The thickness of the sample is read off a dial gauge mounted at the top of the push-rods. The lower part of the assembly can be inserted in a dedicated furnace to control the temperature of the sample. The accuracy of the device is ±10 µm in a temperature range of 0…700 °C. For more details on the test equipment, see [67]. The high stress (>1 MPa) measurements were carried out using commercially available fatigue testing devices (e.g. Instron 8801).

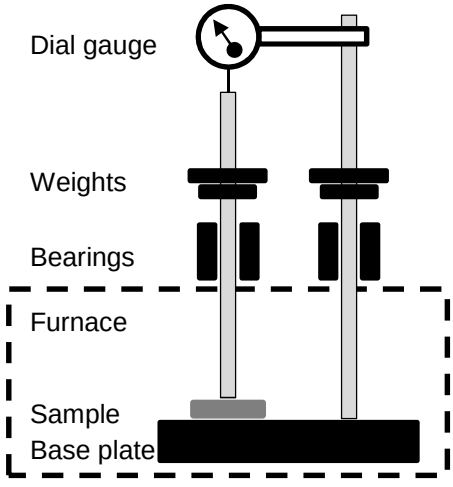

Figure 8. Schematic of the measurement setup

3.3 Results

The thickness of different materials as a function of compressive stress was analysed. Figure 9 shows the effect of temperature on the compressibility of Thermiculite CL87. It can be noted that heating the material significantly reduces the compressibility: already at 200 °C, the compressibility is the same as at 700 °C. If the compressive stress is applied at room temperature before the first heat up, Thermiculite CL87 compresses about 42% between 0.1…0.9 MPa. If full compression to 1.0 MPa is applied after first heat up, the compressibility between 0.1…0.9 MPa is limited to 4%. Most probably the loss of compression is related to drying of the sealing material, and therefore it is likely that any heating above room temperature will result in partial loss of compressibility. Therefore, it is very beneficial to carry out as much of the first compression as possible at room temperature before first heat up. This would allow for the maximum amount of deformability in the sealing materials, therefore allowing for the highest ability to compensate for stack manufacturing and assembly tolerances, leading to a gas-tight stack with low electrical contact resistances.

To compare mechanical properties of Thermiculite CL87 to conventional compressible sealing materials, Figure 10 shows the compressibility of Statotherm HT (phlogopite mica paper) material. It can be noted that this material only compresses about 3% per megapascal of applied stress. This leads to the conclusion that any significant amount of compressibility requires a compressive stress of several megapascals.

Figure 11 shows Schott GM31107 glass sealing material thickness as a function of temperature and time using two different heat-up procedures. The grey curve corresponds to heating under 0.44 MPa of compressive stress, and the black curve to heating under no compressive stress. The weight of the measurement rod corresponds to 0.04 MPa of compressive stress on the sample, so this is the actual stress in a “no compression” case. It is noticed that there is only very little thickness change until about 570 °C. Above that temperature, two distinct changes are noticed, the first at 570…615 °C and the second at 660…700 °C. It should be noted that these are furnace temperatures, so the temperature of the sample lags behind during heating. Based on hot-stage microscopy data [46], the first of these changes relates to binder burnout and sintering, and the second change to glass softening and wetting of the surfaces. The final thickness of the glass was about 12 µm at 0.44 MPa. Further compression to 1.0 MPa at 700 °C did not reduce this thickness. The difference throughout the heating using 0.44 MPa of compressive stress and no stress at all is minimal. Based on these results, the behaviour of the Schott GM31107 glass does not depend greatly on the compression procedure during first heat up. However, if a significant amount of compression is applied at room temperature where the glass tape is very thick compared to its final thickness, the stress distribution within a stack structure should be analysed to be sure that stresses are within acceptable limits.

The methodology and results presented here and in articles I-III are directly applicable to designing SOFC stacks. In the past, methods such as hot-stage microscopy have often been used to gain information on the mechanical properties of glass materials. While this is a reliable method, it is very remote from the actual SOFC stack environment: there is only one (bottom) surface for the glass to wet, no compressive stress, and usually large glass samples are used. With the methodology presented in publications I-III, the measurements are closer to stack conditions: the compressive stress can be varied, the glass has two surfaces to wet, and sample sizes can be realistically dimensioned. The same arguments apply naturally for measuring compressible seals. The measurement data also shows that there is a significant difference in the compressibility of Thermiculite 866 as a function of temperature, which should be taken into account in the assembly and first heat up of stacks.

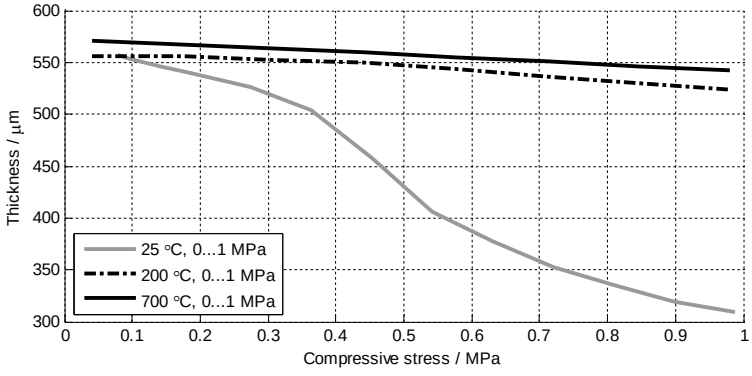

Figure 9. Compressibility of Thermiculite CL87 at room temperature, 200 °C, and 700 °C.

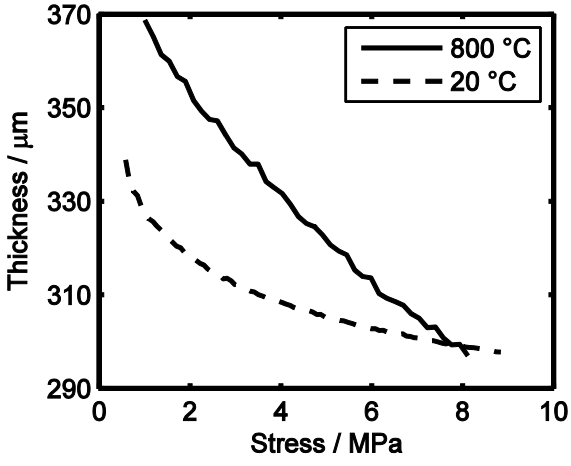

Figure 10. Thickness of Statotherm HT as a function of compressive stress.

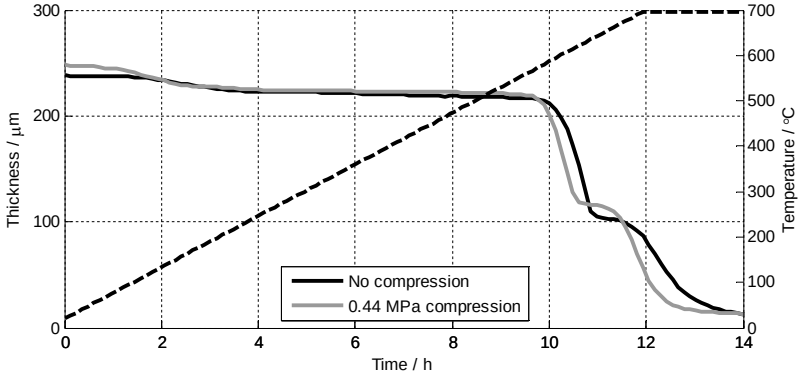

Figure 11. Thickness of Schott GM31107 glass seal (250 µm green tape) as a function of temperature with no compression (0.04 MPa) and with 0.44 MPa compression.

4. Analysis and reduction of stack leakages

4.1 Background

Any fuel burning before the electrochemically active cell does not take part in the electrochemical reactions and therefore decreases the electrical efficiency of the stack. Therefore, reducing leakages is beneficial, as it directly enhances the electrical efficiency of the stack. Leakages can also induce hot-spots or local fuel or air starvation inside the stack. These can cause re-oxidation of the anode or material degradation thus decreasing stack performance and lifetime. Cross leakages between anode and cathode also have an effect on the oxygen to carbon ratio at fuel side, which needs to be taken into account in the process control system. Monitoring leakages through testing is also important, as it gives insight into the lifetime of the seals. In Publication IV, the methodology for ex-situ and in-situ leakage measurements and calculations is presented.

Reducing the required surface stress of the seal diminishes the necessary compression of the stack, which in turn leads to simpler and less expensive compression systems. This also allows more freedom for the stack designer, as thinner, less robust components such as interconnects can be used. A general problem with compressible seals is that lowering the compressive stress increases the leak rate, as the leakage paths along the interfaces tend to dominate the total leak rate. Therefore, using glass seals at low compressive stresses has been a common solution. However, glass seals are usually more difficult to handle and assemble, and require a specific heat treatment procedure. Their electrical resistivity is also usually lower compared to compressible seals, and can be more easily affected by chemical reactions between the glass and adjacent components [68]. Glass seals are also prone to cracking due to thermomechanical stresses generated during thermal cycling [69]. To overcome these challenges, a solution known as a hybrid seal has been presented. In this type of seal, a substrate such as mica paper and conformable interlayers are brought together to form a composite seal. The purpose of the substrate is to provide mechanical properties comparable to compressible seals, while the conformable interlayers diminish interfacial leak-

ages. In Publications III and IV, a glass-based coating was developed to suppress interfacial leakages.

4.2 Experimental

4.2.1 Surface coating

The goal of the experimental work was to design a sealing material that could be operated at low compressive stress (<1 MPa) while still maintaining a leak level below 1% of the stack inlet fuel flow. To this end, a hybrid sealing concept with compressible core substrate and compliant surface layers was chosen. The substrate material for the seal was chosen to be Thermiculite 866, manufactured by Flexitallic Ltd. The glass layer was chosen to be very thin (<20 µm) so that the seal would inherit its mechanical properties from the Thermiculite 866 rather than the glass layer. A thin glass layer also allows the glass to have low viscosity, which helps to seal the interfaces. The glass powder was suspended in an organic carrier consisting of terpineol, ethanol, and ethylene cellulose. Table 3 contains the typical compositions of the coating. By mechanical coating means, the organic content and the viscosity of the suspension were tailored to be much higher (~40 cSt) than when using spray coating (14 cSt) [70]. The results presented here were obtained with a spray-coating method using a U-POL Maximum HVLP mini spray gun with a 1.0 mm nozzle. After applying the coating, the coated Thermiculite 866 sheets were dried at 75 °C for 2 h and then cut to the required shape. All the seals were heated from room temperature up to 700 °C using a 60 $°Ch^{-1}$ ramp rate. For more details on the coating process, see [71] and [72], and for more details on the mechanical properties of the coated seals, see [67].

Table 3. Typical compositions of various coatings.

Coating method	terpineol / w%	ethanol / w%	ethyl cellulose / w%	Glass to organic – ratio / w/w	Viscosity / cSt
Brush/spatula/roller	81	15	4	2:1	40
Wet spraying	24	75	1	1:2	14

4.2.2 Leak rate measurements

Leak rate measurements were conducted on the manufactured hybrid seals, as well as for the non-coated core material (Thermiculite 866). Ring-shaped seals of 40 mm outer diameter and 5 mm landwidth were placed between Crofer 22 H plates (Figure 12). The bottom plate was 20 mm thick and the top plate 1 mm thick. The gas was fed into the seal via a hole in the middle of the bottom plate. A chosen gas flow was fed to the seals with mass flow controllers, and a pressure controller kept the gas pressure at a set level.

After heat up in air, the samples were exposed to 50/50 H_2/N_2. Leak rate measurements were conducted periodically by closing the valve V1 and logging the pressure decay. The leak rate measurement and calculation procedure were based on measuring the pressure decay and calculating the leak rate as a function of pressure from that. For more details on the methodology, see Chapter 4.3.

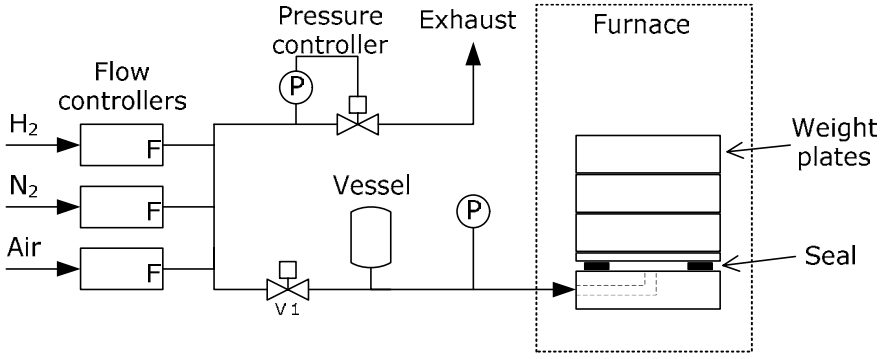

Figure 12. Leak test setup.

4.2.3 Stack test

To further verify the sealing solution, a test stack was manufactured and tested. The stack contained 30 cells by Elcogen AS. Table 4 presents the main features of the stack. Figure 13 shows a picture of the stack before the start of the test. The pipe coils at the bottom provided pre-heating for the air and fuel. The two vertical rods at the right are the current rods. Compression was provided through the thick vertical pipes at the bottom and top of the picture. The smaller pipes at the left are the impulse lines of the pressure transducers.

During heat up, air was fed to both the anode and cathode sides of the stack, to ensure that all the organic binders of the coating on seals were burned off. After heat up, the anode side was reduced with hydrogen in nitrogen. Cross leaks were measured before reduction, after reduction, and during operation.

Table 4. Nominal operating conditions of the stack.

Cells	30 pcs Elcogen ASC-10B
Flow configuration	Co-flow
Active area	81 cm^2
Cathode inlet temperature	590 °C
Cathode outlet temperature	700 °C
Current density	0.25 Acm^{-2}
Air utilization	22%
Fuel utilization	46%
Cathode outlet pressure	ambient
Flows during heat up	Anode: 4.5 NLPM air Cathode: 4.5 NLPM air
Flows before reduction	Anode: 4.5 NLPM N_2 Cathode: 4.5 NLPM air
Flows at OCV	Anode: 0.5 NLPM H_2, 8.5 NLPM N_2 Cathode: 8.5 NLPM air
Flows at nominal operating conditions	Anode: 9.0 NLPM H_2, 8.5 NLPM N_2 Cathode: 50 NLPM air

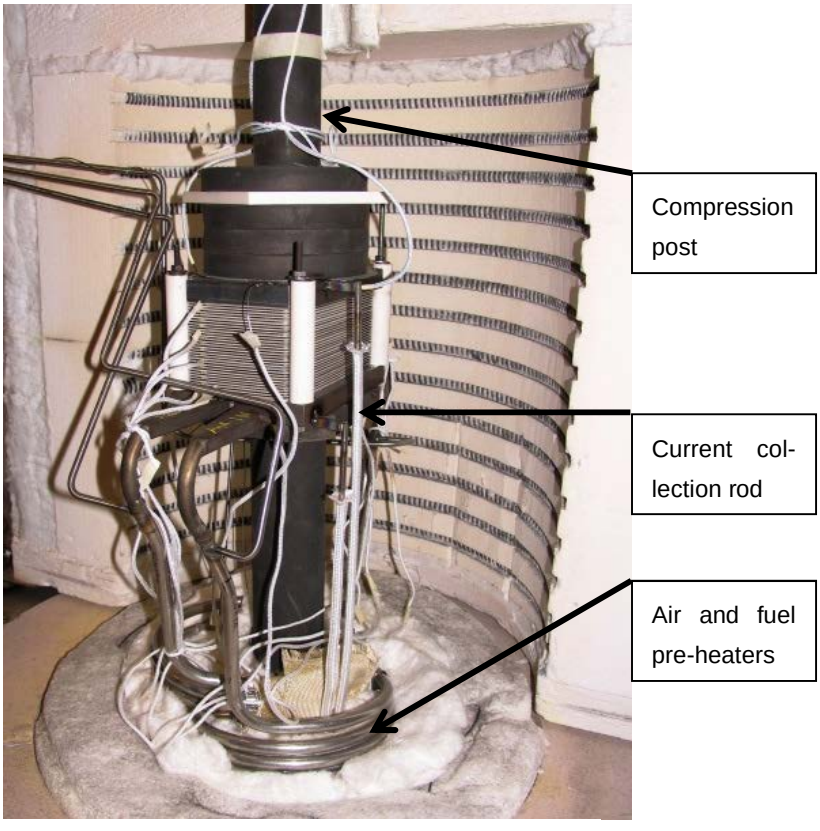

Figure 13. The 30-cell stack in a furnace before testing.

4.3 Leak rate analysis

4.3.1 Pressure drop methodology

Ex-situ leak test results in this thesis have been calculated by analysing pressure versus time curves while the sample and its associated volume have been isolated. This allows for calculation of the leak rate as a function of pressure between the starting pressure and the end pressure of the decay, resulting in a large amount of data based on a single measurement. Based on the ideal gas assumption, the leak rate is proportional to the slope of the pressure decay curve, and therefore the leak rate can be written as a function of pressure

$$\dot{Q}_{NTP} = V \frac{T_{NTP}}{T p_{NTP}} \frac{dp}{dt} , \qquad (2)$$

where V is the combined volume of the vessel and the sample, T is the average temperature of the gas in the volume, and T_{NTP} and p_{NTP} are normal temperature and pressure.

From the equation above, it can be noted that the accuracy of the result depends on accuracies of volume, temperature, and dp/dt. The volume of the system can be determined with high accuracy, so that can be neglected. The average temperature of the gas inside the system volume is more prone to errors. It is estimated that this error is less than ±15 °C, corresponding to a leak rate uncertainty of 5%. For evaluation of the derivative dp/dt, there are several options. If one wants to calculate leak rate at a specific pressure from the data, which is a set of points taken at regular intervals, one could approximate dp/dt by a difference in pressure and time of the consecutive steps

$$\frac{dp}{dt} \cong \frac{p_i - p_{i-1}}{t_i - t_{i-1}} . \qquad (3)$$

If the sampling rate has been sufficient, the difference p_i-p_{i-1} is bound to be small. Therefore, any random uncertainty of the pressure measurement will induce a large relative error in the pressure measurement. To overcome this, a third degree polynomial was fitted to the pressure versus time data using the least squares method, thus minimizing the random uncertainty of the pressure measurement. The fitted polynomial was then differentiated to obtain the leak rate as a function of pressure. Figure 14 presents this methodology in graphical format. On the top left, there is raw pressure data and below it, there is leak rate as a function of pressure, calculated using consecutive points in the data (the equation above). It can be noted that even a small amount of noise in the pressure data results in very noisy leak rate data. On the top right is the same pressure data fitted with a third degree polynomial, and below it is leak rate as a function of pressure, calculated

by differentiating the polynomial. The resulting data through this processing method is much more usable.

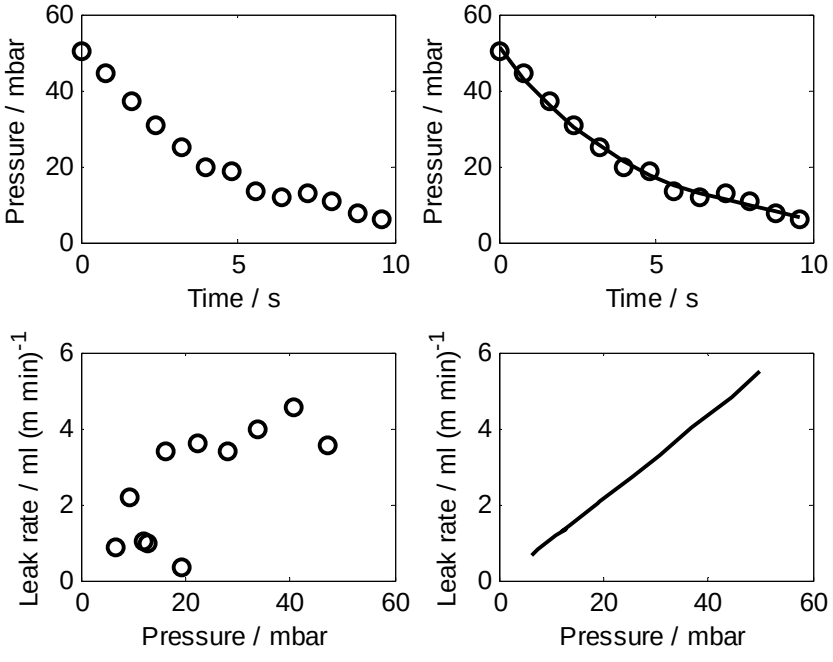

Figure 14. Example of the pressure decay methodology. Leak rate calculated using individual data points (left) and polynomial fit (right).

4.3.2 Stack tests

During stack tests, cross leak between anode and cathode is an important parameter to monitor. An increase in cross leak directly decreases electrical efficiency and it may also be an indication of a developing mechanical failure such as a cracked cell or seal. An easy way of measuring cross leak is to observe the open circuit voltage (OCV) and compare this value against the theoretical value given by the Nernst potential

$$E = -\frac{\Delta G}{2F} + \frac{RT}{2F}\ln\left(\frac{p_{H2}p_{O2}^{0.5}}{p_{H2O}}\right), \quad (4)$$

where ΔG is the change of Gibbs energy, F is the Faradic constant, R is the gas constant, T is the temperature and terms denoted with p are partial pressures of the reactants. This is only applicable at OCV and not during operation. It should also be noted that any leak taking place after cell cannot be detected with this method. Figure 15 presents theoretical Nernst potential as a function of anode side humidity (induced by cross leak of oxygen) and temperature. As cell voltage can easily be measured accurately, and cell temperature is also usually known at OCV, at least within 100 °C, this method can be used for a rough check on the leakages. For example, a cell voltage of 1.2 V at 700 °C yields a humidity of 0.2% at the anode. It should be noted that since according to

$$H_2 + \frac{1}{2}O_2 \rightarrow H_2O \quad (5)$$

only half a mole of oxygen is needed per mole of steam. Therefore, 0.2% steam content at the anode corresponds to 0.1% of leaked oxygen molecules compared to anode inlet flow.

In the stack test presented in this chapter, cross leakages were quantified by measuring steam and oxygen content from cathode and anode outlets. Oxygen cross leak was calculated before cell reduction as

$$\dot{Q}_{O_2}^{cross} = X_{O_2}^{A,out}\dot{Q}_{N_2}^{A,in}. \quad (6)$$

By this methodology, one is able to measure the stack cross leak before introducing reducing gases (hydrogen) to the stack. The hydrogen cross leak after reduction was calculated as

$$\dot{Q}_{H_2}^{cross} = (X_{H_2O}^{C,out} - X_{H_2O}^{C,in})(\dot{Q}_{air}^{C,in} - n_{cells}\frac{I}{4F}\frac{RT_{ntp}}{p_{ntp}}), \quad (7)$$

where terms denoted with X are measured oxygen and steam volumetric fractions, n_{cells} is the number of cells in the stack (30), I is the current drawn from the stack, and F is the Faradic constant. These calculations are based on the assumption

that the leak rates between ambient and anode/cathode and the nitrogen cross leak are small compared to total flow rates.

As partial pressure measurements of oxygen and steam at stack outlets can be used in all operating conditions, these were used as a primary means to assess stack leakages.

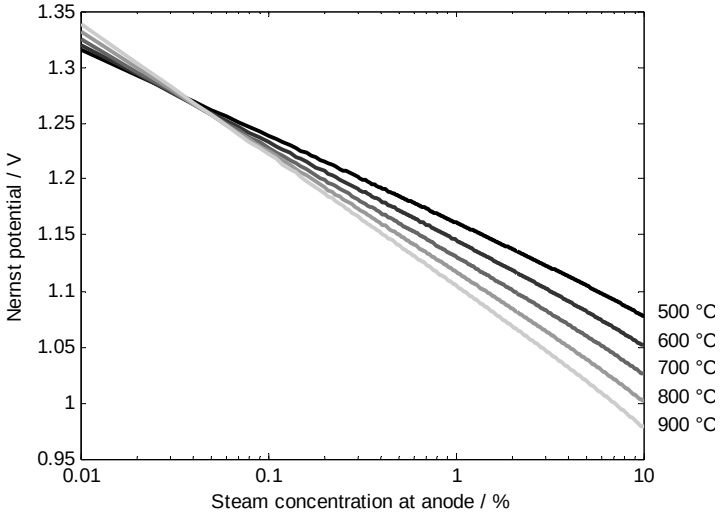

Figure 15. Nernst potential of 50/50 H_2/N_2 fuelled fuel cell as a function of temperature and anode steam concentration (leak).

4.4 Results

4.4.1 Surface coating

Hybrid seals were manufactured by coating glass layers with an organic carrier on top of compressible Thermiculite 866 substrate. Figure 16 shows a SEM cross-section of Crofer 22 APU / seal / Crofer 22 APU structure after heat-treating 50 h at 700 °C. It can be noticed that the glass interlayers are well adhered to the Thermiculite structure, even penetrating slightly in between vermiculite/steatite slits. Figure 17 shows another cross-section of the coated seal. The bottom steel plate had been intentionally scratched before assembly with ~15 µm scratches, to observe the filling properties of the coating. It can be noted that the glass coating has filled the scratch fully and formed clearly a gas tight seal also in this area.

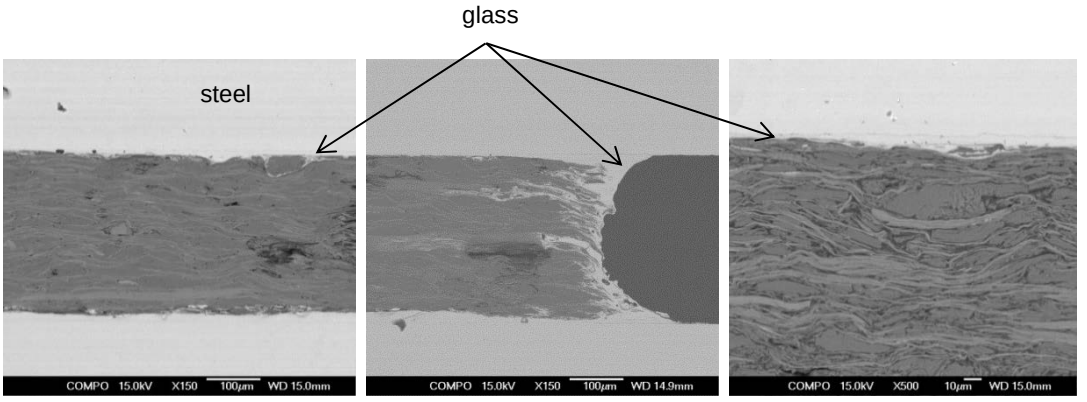

Figure 16. SEM cross-sections of the manufactured seals.

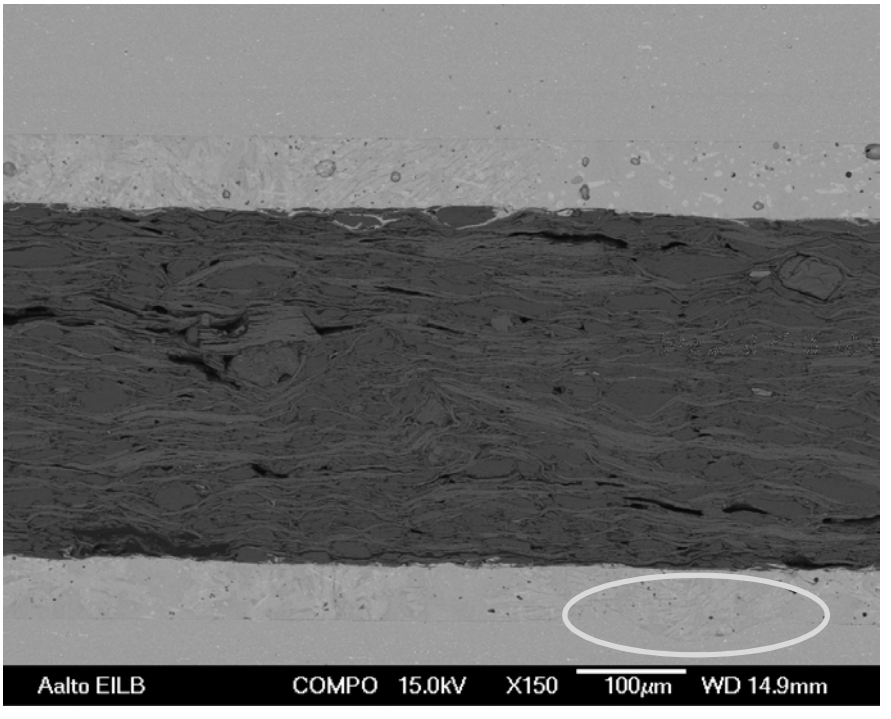

Figure 17. Cross-section of coated seal. Scratches in the Crofer 22 APU have been filled.

4.4.2 Ex-situ leakage tests

Leak rates of the manufactured hybrid seals and of core material (Thermiculite 866) were measured. Figure 18 presents leak rates of the samples as a function of gas pressure at 0.1 MPa and 0.4 MPa compressive stresses. From this figure, it can be noticed that the surface coating decreases the leak rate of Thermiculite 866, especially at low compression stress levels. The coated Thermiculite 866 seals show leak rates of 0.1…0.3 ml (m min)$^{-1}$, which is a reduction of 60…90% compared to uncoated samples, which showed leak rates of 0.3…3 ml (m min)$^{-1}$.

Figure 19 shows the leak rate as a function of pressure using different test gases. There is a difference in slopes of the leak rate versus pressure curves between coated and uncoated samples. The coated samples show almost constant leak rate as a function of pressure with H_2/N_2 mixtures, while leak rates of uncoated samples are more pressure dependent. This suggests that with the coated samples, the primary driving force is concentration gradient rather than pressure gradient, as with the uncoated samples. The negligible dependency of the overpressure on the diffusive leak rate can be understood by considering Fick's law of diffusion, using total concentration c_{TOT}, total pressure p_{TOT}, and the molar fraction x:

$$J = -D\nabla c = -c_{TOT} D\nabla x = -\frac{p_{TOT}}{RT} D\nabla x \qquad (8)$$

where D is diffusion coefficient, c is concentration, x is fraction, p is pressure, R is the gas constant and T is temperature. From this equation, one can notice that varying the absolute overpressure p_{TOT} in a range of ~1000…1030 mbar induces very little effect on the concentration-driven leak rate. Although the real situation is more complex, the concentration dependency of the leak rates should be carefully considered, as different research groups use very different gas compositions and overpressures for leak tests, such as 3% H_2 in nitrogen or argon, 100% H_2 or 100% He.

The effectiveness of the surface coating was further tested by thermally cycling the seals and observing leak rates. Figure 20 shows the leak rate data before and after five thermal cycles for coated and uncoated seals. The leak rate of the hybrid seal remains stable at around 0.2 ml/m/min level at 25 mbar overpressure, while the uncoated seal shows a leak rate of about 3 ml/m/min. It can be noticed that the leak rates of the compressible and hybrid seals do not change during thermal cycling, and the leak rate of the hybrid seal is about 90% less than that of the compressible seal.

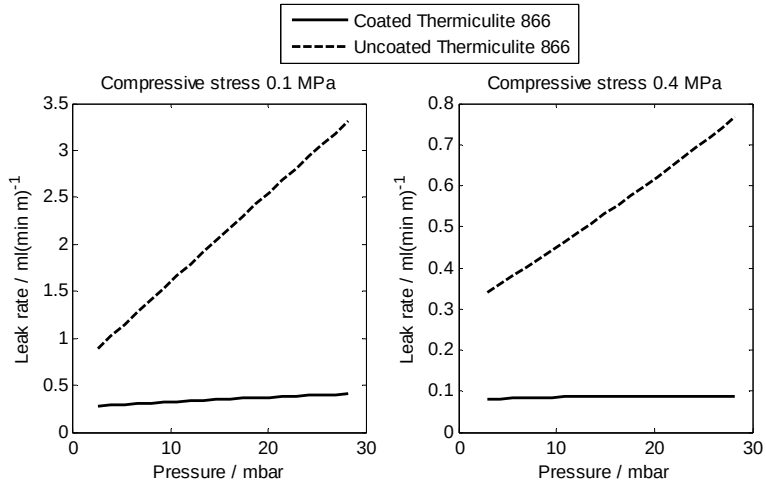

Figure 18. Leak rate comparison of coated and uncoated seals (50/50 N_2/H_2).

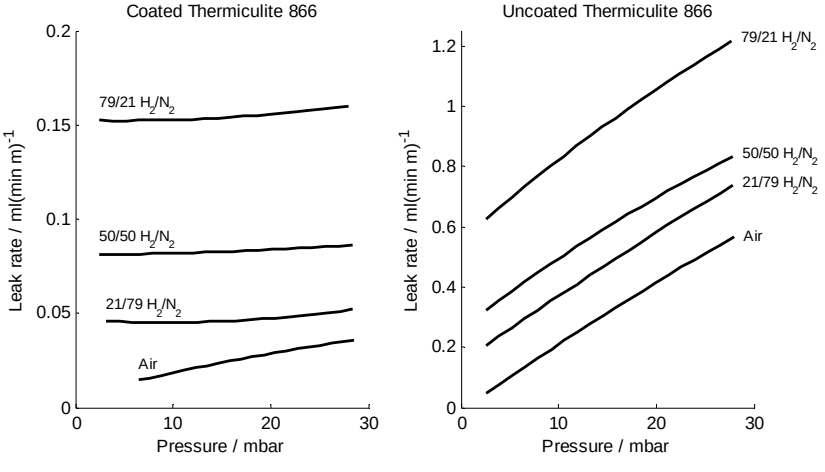

Figure 19. Leak rate comparison of coated and uncoated seals with different gas atmospheres.

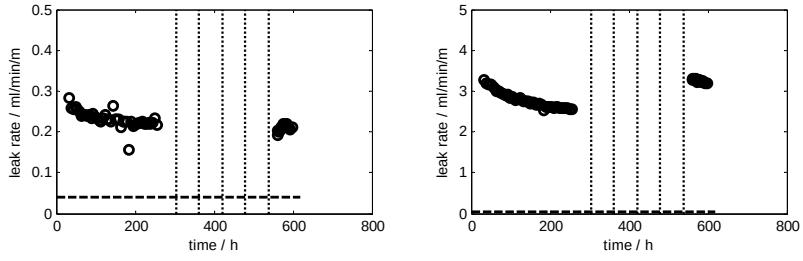

Figure 20. Leak rates of coated seal (left) and uncoated seal (right) before and after five thermal cycles.

4.4.3 Stack test

A 30-cell stack was assembled and tested using the manufactured hybrid seals. The oxygen cross leak of the stack was measured before reduction, and hydrogen cross leak at purge gas and during operation. Table 5 shows the calculated leak rates in different operating conditions, along with the measured quantities. The hydrogen leak rates have been analysed by measuring steam concentration at cathode out. The oxygen leak has been analysed by measuring oxygen concentration at anode out before reduction, and by measuring OCV at 50/50 H_2/N_2. It can be noted that leakages with air and with 5% hydrogen in nitrogen mixture (purge gas) are significantly lower than with higher hydrogen concentration (nominal operating conditions). This is further illustrated in Figure 21, where hydrogen cross leak of the 30-cell stack is plotted as a function of average hydrogen concentration between anode inlet and outlet. It can be observed that the leak rate is directly proportional to the hydrogen concentration. This behaviour corresponds well with the ex-situ observations presented in the previous chapter. The hydrogen cross-leak at nominal operating conditions corresponds to about 0.7% of inlet hydrogen flow, which is well below the 1% target set for this thesis work.

Table 5 also contains leak rates per unit length, allowing comparison between leak rate tests. During nominal operating conditions, the hydrogen cross leak was 4 ml/m/min. In this condition, anode gas composition was 49% H_2 in N_2, which is almost identical to the 50/50 H_2/N_2 mixture used in most of the ex-situ tests. At 0.1 MPa of compressive stress, ex-situ tests showed leak rates of 1…3 ml/m/min, and at 0.4 MPa of compressive stress the leak rates were 0.3…0.8 ml/m/min. It can be noted that the stack leakages and values measured fall in the same order of magnitude. The difference between these values could be explained by inhomogeneous stress distribution on the stack seals.

Table 5. Summary of the measured leak rates and flow rates. The cathode inlet humidity was constant at 0.08%.

	Direction of leak	Measured quantity	Calculated leak	
			ml min^{-1}	ml (m $min)^{-1}$
Before reduction	Ambient, cathode => anode	0.18% O_2 (anode out)	8±2 (O_2)	0.3±0.1
Purge gas	Anode => cathode	0.20% H_2O (cathode out)	10±2 (H_2)	0.7±0.2
OCV (50/50 H_2/N_2)	Ambient, cathode => anode	Average cell volt-age 1163 mV	46±15 (O_2)	1.5±0.5
Nominal	Anode => cathode	0.20% H_2O (cathode out)	60±12 (H_2)	4±0.9

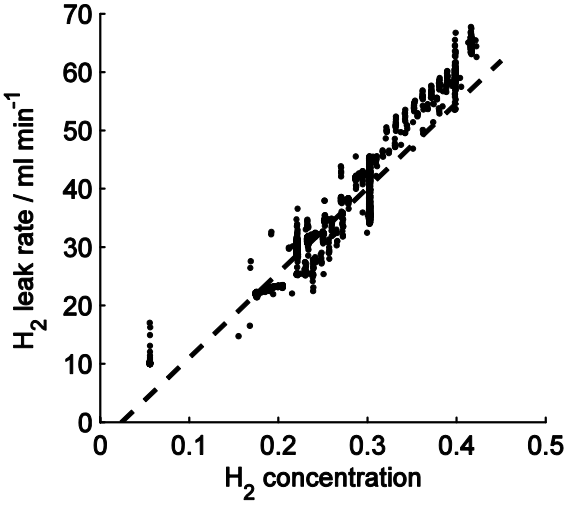

Figure 21. Hydrogen cross leak of the 30-cell stack as a function of average hydrogen concentration between anode inlet and outlet.

5. Analysis of corrosion phenomena and protective coatings in SOFC stacks

5.1 Background

The high operating temperatures of SOFC stacks in combination with both oxidizing and reducing atmospheres presents a challenging environment for materials. Corrosion of materials can take place due to interfacial reactions as well as by gas/solid reactions. Of special importance is to avoid any corrosion mechanism that can lead to deactivation of the electrochemical cell. One typical example of these deactivation mechanisms is chromium evaporation from interconnect steel materials. The evaporated chromium is transported in the gas phase to the electrochemically active cell, where it can solidify to chromium oxide, causing loss of performance [73]. The transported chromium can also react with strontium in SOFC cathode materials and for strontium chromate ($SrCrO_4$). The electrical resistivity of strontium chromate is in the order of 60 Ωm at 800 °C and increases with decreasing temperature [74]. This corresponds to area-specific resistivity of 0.6 Ωcm^2 at a thickness of only 1 µm. Therefore, it is clear that formation of strontium chromate can cause significant ohmic losses in stack performance. These phenomena can be mitigated with, for example, chromium barrier coatings on interconnect steels. A variety of protective coatings are reported in the literature, see e.g. review of Shaigan et al [75]. Coatings based on $(Mn,Co)_3O_4$ spinels have been of high interest due to their good performance, see e.g. [76]. More recently, $MnCo_{2-x}Fe_xO_4$ has been tested for its' higher electrical conductivity [77].

Publication V deals with development and application of a protective coating for SOFC interconnects. Publication VI presents corrosion analysis of different interfaces within a stack.

5.2 Experimental

5.2.1 Manufacturing of protective coatings

To mitigate effects of chromium evaporation from interconnects, two different protective coatings were prepared and tested. The first one was manufactured from a commercially available $MnCo_2O_4$ powder, and the second one ($MnCo_{1.8}Fe_{0.2}O_4$) was manufactured in-house via a solid carbonate synthesis route. The coatings were deposited on Crofer 22 APU plates by a high-velocity oxygen flame (HVOF) method. See [78] for more details on the HVOF process. As using thin, formed steel interconnects is of interest from a cost savings point-of-view, coatings were also deposited on corrugated 0.2-mm-thick Crofer 22 APU coupons. Figure 22 presents a schematic of the test setup for analysing the mechanical properties of the manufactured coatings on top of corrugated steel plates. These plates had a corrugated area of 34x34 mm^2, and a force of 50 N was applied on top of the assembly. See [38] for more details on sample preparation.

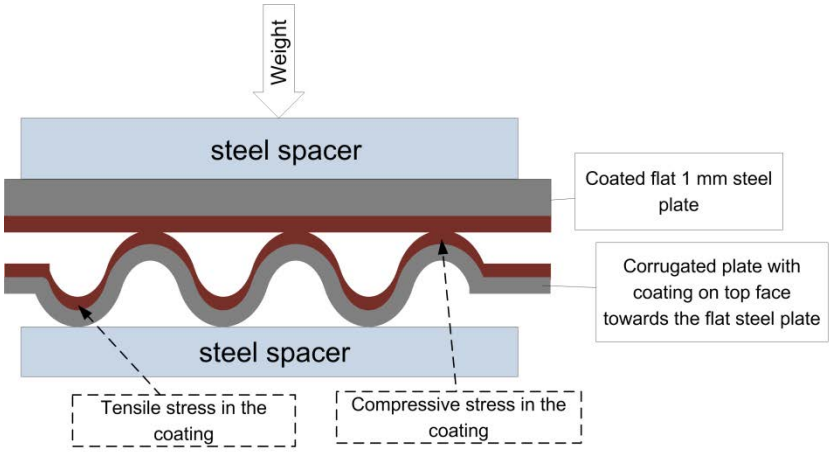

Figure 22. Protective coatings were deposited on corrugated steel coupons to analyse the effects of tensile and compressive stresses on the coating.

5.2.2 Area-specific resistance measurements

To evaluate the electrical performance of different chromium protective coatings, area-specific resistance (ASR) measurements were conducted on coated and uncoated steel plates. Two different coatings ($MnCo_2O_4$ and $MnCo_{1.8}Fe_{0.2}O_4$) were applied on flat steel plates and tested. Figure 23 shows the experimental setup of the ASR measurements. Plates were stacked into a tower, and $La_{0.85}Sr_{0.15}Mn_{1.1}O_3$ (LSM) spacers (IRD Fuel Cells A/S, Denmark) were inserted between samples to mimic the contact between the interconnect and cathode in the SOFC stack. Wires for voltage measurements were connected to the samples and current feed wires at the end of the tower. Current density in these measurements was 0.2 A/cm^2, which corresponds to the typical current density of an SOFC stack. A vertical load of 20 N was applied on the 20x20 mm^2 samples. The steady state measurements were conducted in dry air at 700 °C for 1000 h.

In order to avoid lateral current flow in the samples, the resistance of the samples needs to be significantly higher than that of the steel spacers. Resistivity of Crofer 22 H is about 1 µΩm, whereas resistivity of chromium oxides is of the order of 0.1…1 Ωm [29]. This difference of 5…6 orders of magnitude ensures that the current flow in the samples is perpendicular to the plane. Area specific resistances were calculated using

$$ASR = \frac{UA}{I}, \qquad (9)$$

where U is voltage, A is sample area and I is current. Error estimate for the ASR can be calculated as

$$\Delta ASR = \frac{A}{I}\Delta U + \frac{UA}{I^2}\Delta I + \frac{U}{I}\Delta A = ASR\left(\frac{\Delta U}{U} + \frac{\Delta I}{I} + \frac{\Delta A}{A}\right) \qquad (10).$$

Majority of the error originates from the ΔA/A terms which denotes the placement error of samples on top of each other. The measurement accuracies were 5 µV, 0.5 mA and 0.5 cm^2. Therefore the total uncertainty of the ASR measurement is about 10%.

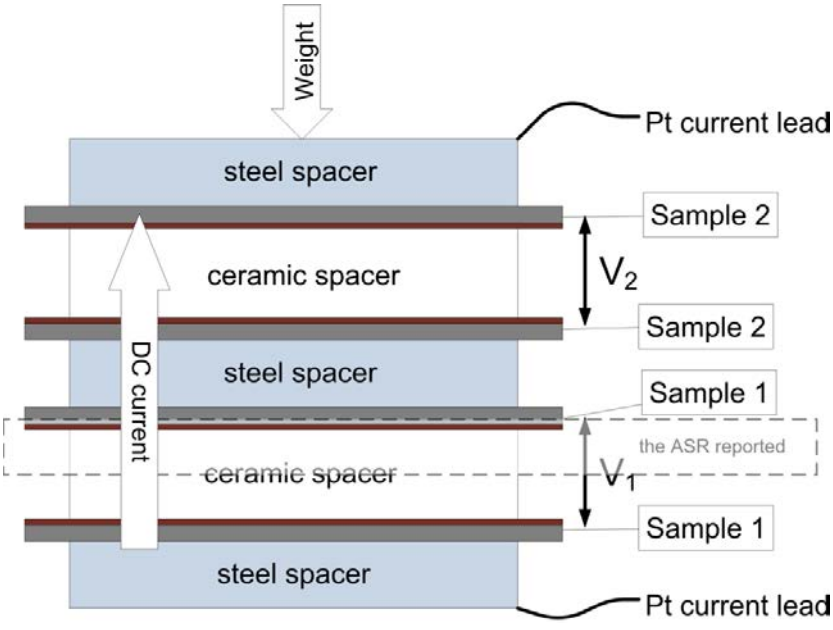

Figure 23. Setup for the ASR measurements.

5.2.3 Stack tests

To study corrosion phenomena in real SOFC stack operating conditions, two single cell stacks were manufactured. Table 6 provides information on the main components of the stacks used in these corrosion studies. The main purpose of stack one was to verify the effectiveness of the $MnCo_{1.8}Fe_{0.2}O_4$ spinel coating in suppressing chromium evaporation from the interconnect steels. The interconnect plates were manufactured from 1-mm-thick Crofer 22 APU steel and the gas channels were etched onto interconnects. A 20-µm-thick layer of $MnCo_{1.8}Fe_{0.2}O_4$ coating was sprayed with HVOF on the cathode side of interconnects. The stack was operated with hydrogen and air for 6000 h at 700 °C.

The main purpose of stack two was to study possible material interactions between sealing materials and interconnect steels. Seals for this stack were of a hybrid type consisting of compressible Thermiculite 866 core material [63] and glass interlayers. For more details on the sealing configuration, see [71]. The stack was operated for 1800 h at 700 °C with hydrogen and air. The effectiveness of the chromium barrier coating was also analysed.

Table 6. Main components of the two single cell SOFC stacks used in corrosion studies.

Stack	Cells	Inter-connects	Coatings	Coating method	Seals	Temp / °C	Duration / h
1	Anode supported Ni/YSZ/LSCF	Crofer 22 APU, d=1 mm	$MnCo_{1.8}Fe_{0.2}O_4$ (~20 µm)	HVOF	Thermiculite 866	700	6000
2	Anode supported Ni/YSZ/LSCF	Crofer 22 APU, d=0.2 mm	None	None	Thermiculite 866 + Schott GM31107 glass tapes	700	1800

5.3 Results

5.3.1 Mechanical properties of protective coatings

Protective coatings were first manufactured on top of flat and corrugated steel plates to analyse mechanical strength, adherence, and coverage of the layers. Figure 24 shows cross-sections of $MnCo_{1.8}Fe_{0.2}O_4$ coating on a flat Crofer 22 APU steel plate after 1000 h exposure in air at 700 °C. It can be noted that the coating is dense with only about 5% of closed porosity. The thickness of the chromium oxide layer on top of the steel is about 0.5 µm, which is a good result compared to a non-coated control sample, which showed an oxide layer of about 3 µm. Therefore, it can be concluded that the coating effectively reduces oxidation of the interconnect, thus prolonging its lifetime.

Figure 25 shows cross-sectional SEM images of the $MnCo_2O_4$-coated corrugated plate. It can be noticed that at both the top and the bottom of the groove, the coating is homogeneous and dense, with only about 5% of closed porosity. The image on the left (the top of the groove) shows that the coating has been able to withstand the compressive stress. In the right image (the bottom of the groove), small fractures can be noticed, suggesting that the tensile stress present in this location has caused fractures in the coating.

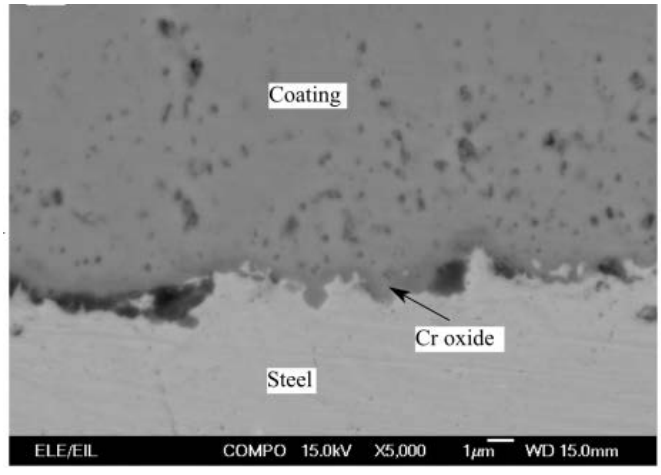

Figure 24. BSE SEM image $MnCo_{1.8}Fe_{0.2}O_4$ coating on Crofer 22 APU substrate exposed to air at 700 °C for 1000 h.

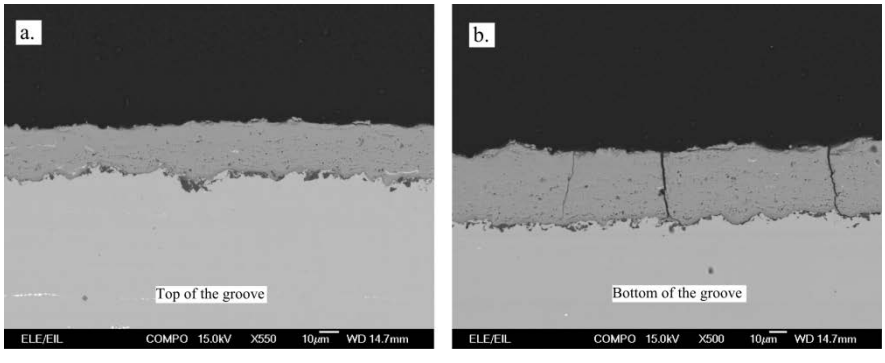

Figure 25. SEM images of $MnCo_2O_4$ coating deposited on top of corrugated Crofer 22 APU plates (Figure 22) after 1000 h exposure in air at 700 °C. Left: top of the groove (compressive stress); right: bottom of the groove (tensile stress).

5.3.2 Area-specific resistance measurements

Area-specific resistance measurements were carried out to evaluate ohmic losses associated with steel/cathode interfaces. Figure 26 shows ASRs of coated and uncoated Crofer 22 APU steel plates. It can be noted that both coatings show stable resistances of about 20 mOhmcm^2 throughout the 1000 h test. Resistance of the uncoated Crofer 22 APU plate declines during the test, starting from 100 mOhmcm^2, and shows signs of levelling at the end of the test, at about 50 mOhmcm^2. The decrease of ASR of the uncoated sample is related to the faster oxide layer growth compared to the coated samples. This growing oxide layer widens the actual contact area and therefore decreases the observed contact resistance.

The target for this work was to achieve less than 1% ohmic contact loss between the interconnect and cell. At 0.3 Acm^{-2} current density and 0.85 V cell voltage, this would correspond to an ASR of about 30 mΩcm^2. The coated steels showed ASRs of about 20 mOhmcm^2, which was well below this target.

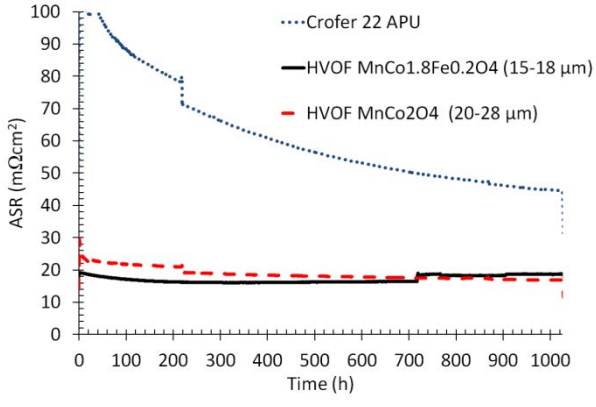

Figure 26. Area-specific resistance of coated and uncoated Crofer 22 APU plates.

5.3.3 Analyses of protective coatings after SOFC operation

The two stacks tested (Table 6) enabled a study of effectiveness of the $MnCo_{1.8}Fe_{0.2}O_4$ coating in preventing chromium evaporation. Figure 27 presents SEM images of the stack one cross section. Figure 27a shows that the coating has been uniformly deposited on the interconnect plate. What is noticeable is that the coating is also thick and dense at the sides of the rib, which are difficult areas for HVOF coating, as they are almost perpendicular to the spraying direction. After 6000 h of SOFC operation, the coating is still dense and the amount of porosity (~5%) is similar to the 1000 h ex-situ test (Figure 25). It seems that there have been no changes in the coating when compared to the 1000 h ex-situ test and the 6000 h SOFC operation tests, which is a good result indicating the stability of the coating. Figure 27b shows a cross-section at the location of the interconnect rib. EDS analyses of this area showed no signs of chromium in the cathode, suggesting that the coating has suppressed the chromium transport to the cathode. Figure 27d shows an EDS line scan of chromium in the middle of the gas channel (no contact with the interconnect). It can be noticed that there is a maximum of about 2% of chromium in the outer/middle part of the cathode furthest away from the electrolyte. To ascertain this result, 19 line scans from this area were measured. As a result, five of these scans showed chromium amounts over the detection limit (~0.3%). Since there was no chromium detected in the cathode area that was against the rib, it must be concluded that the chromium in the channel area has been most probably transported to this location in a gaseous phase. The origin for this chromium could be the uncoated end plates of the stack.

To compare the effectiveness of the chromium barrier coating against uncoated interconnect, the chromium content of the cathode was also analysed at two locations (Figure 28) of stack two. At the air channel location, EDS analysis showed a chromium concentration of 0…2% mostly at the outer surface of the cathode, which is in line with the findings of stack one. However, at the location where the cathode is in contact with the rib, there was as much as 18% of chromium near the contact area. This is a very significant amount compared to the coated stack, which showed no chromium at the cathode in this contact area.

These two stack tests have shown that the chromium evaporation-related corrosion and deactivation mechanisms were mitigated using protective $MnCo_{1.8}Fe_{0.2}O_4$ manufactured with HVOF. There was no noticeable change in the $MnCo_{1.8}Fe_{0.2}O_4$ coating when comparing the 1000 h ex-situ test and the 6000 h tests, suggesting it would be a good candidate in achieving a 10000 h operational lifetime.

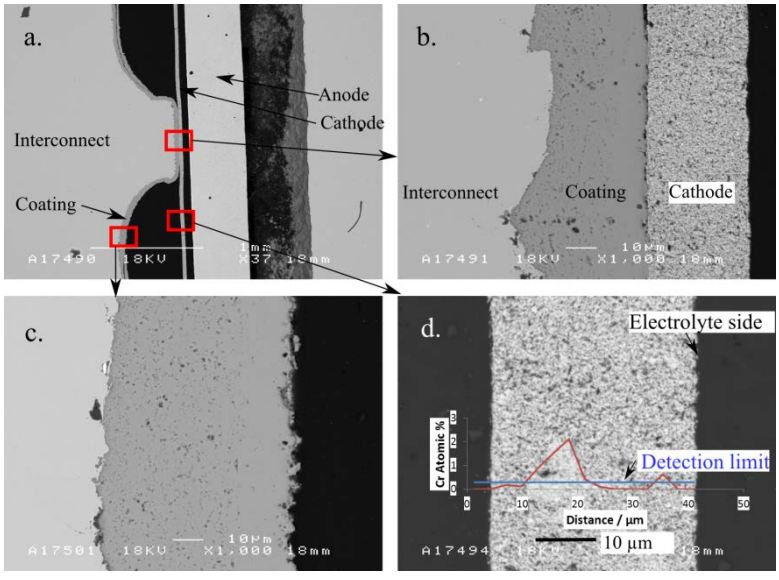

Figure 27. Cross-sectional SEM images of stack 1 with coated interconnects.

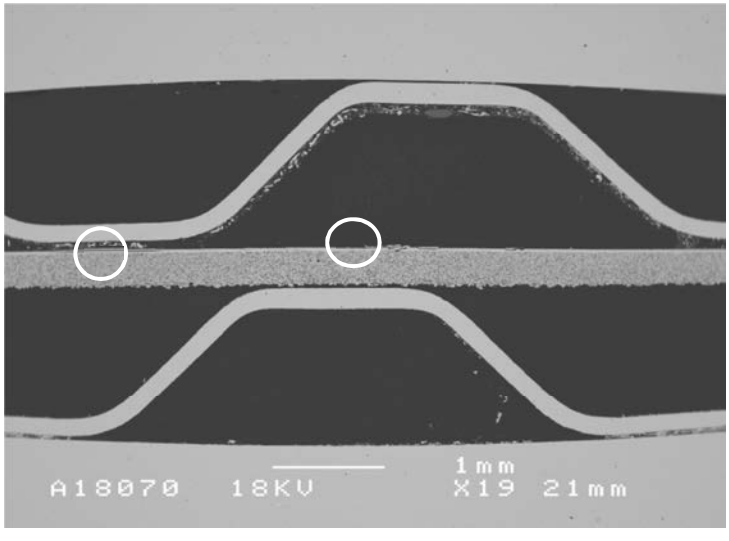

Figure 28. Cross-sectional SEM image of stack two. White circles indicate locations of the EDS analysis. Left: cathode against the interconnect rib; right: cathode at the gas channel.

5.3.4 Analysis of material interaction after SOFC operation

The main purpose of stack two (Table 6) was to study possible material interaction between sealing materials, interconnects, and the cell. Figure 29 shows a SEM image of the seal away from its outer edges, meaning it is only exposed to a gas atmosphere through leakage. The oxide layer thickness on the Crofer 22 APU interconnect is about 1 µm, which can be seen as a good value after 1800 h of SOFC operation. Figure 30a&b shows SEM images of the steel/glass/air triple interface at the upper and lower parts of the same seal. The upper part is free of corrosion, but in the lower location there is a corrosion layer of about 20 µm of thickness, spreading 200 µm from the triple interface. A similar corrosion layer was also found on the bottom of the gas manifold. The bottom of the manifold channel is the most difficult spot to clean before assembly. This suggests that this corrosion effect might have been caused by insufficient cleaning of the plates.

Figure 31 shows a SEM image of the glass/electrolyte interface. The adherence of the glass to the electrolyte is good, and no visible material interaction can be seen.

Figure 32 shows a SEM image of the steel/glass interface exposed to an anode atmosphere. The location is close to the anode outlet, so in addition to hydrogen there is also steam present, due to fuel cell reactions. No material interaction is detectable at this point. The cracks in the glass layer have been caused by the sample preparation.

Corrosion behaviour of interconnects in single and dual atmosphere exposure was also studied with this stack. Figure 33 shows SEM images of interconnects in a fuel/air atmosphere (left) and in an air/air atmosphere (right). In both atmospheres, oxide layer thicknesses are 1…2 µm, and the scales seem dense and well adhered to interconnects. In both exposure conditions, there is a limited amount of inward oxidation, with a depth of 5 µm. There are no signs of detrimental corrosion, which is a good result considering that the interconnects were not coated.

The hybrid seal developed in this work did not cause unwanted corrosion at the interfaces of sealing during 1800 h of testing. Therefore, it can be concluded that these material solutions have the potential to be used in SOFC stacks in long-term operation.

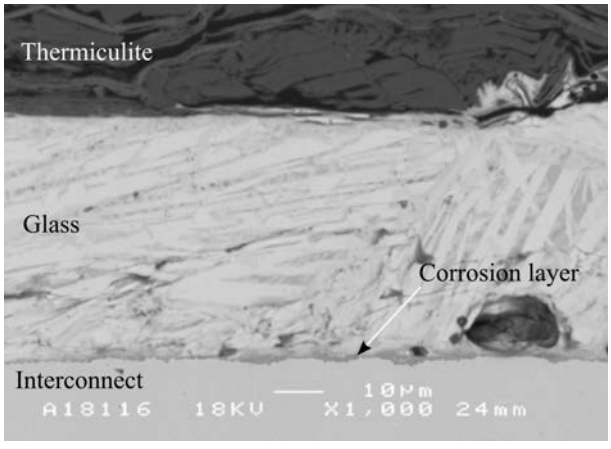

Figure 29. SEM-image taken in the middle of the seal, away from the outer faces.

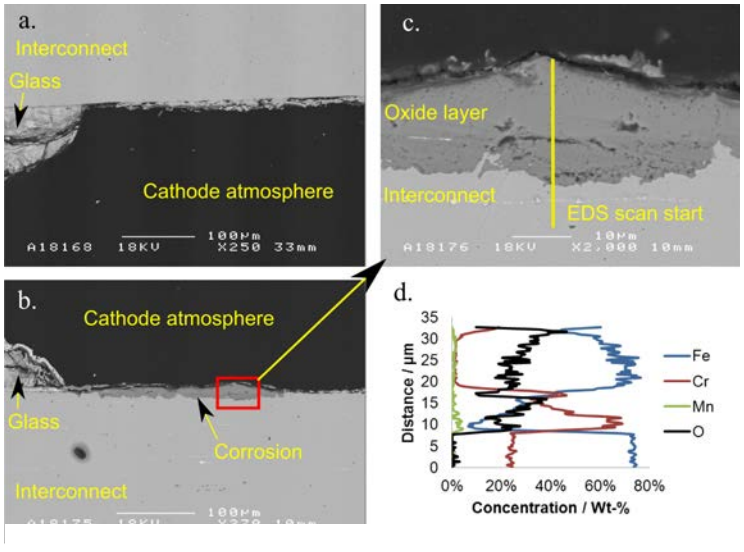

Figure 30. SEM cross-sectional images of steel/glass interfaces exposed to a cathode atmosphere.

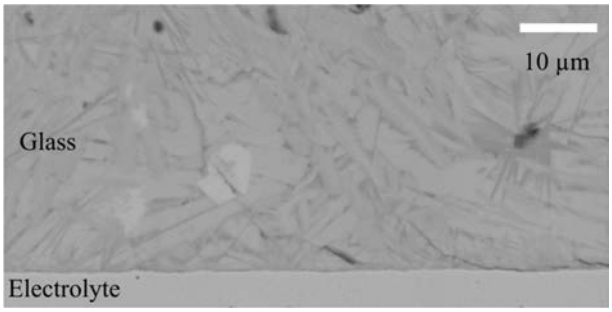

Figure 31. SEM image of the glass/electrolyte interface.

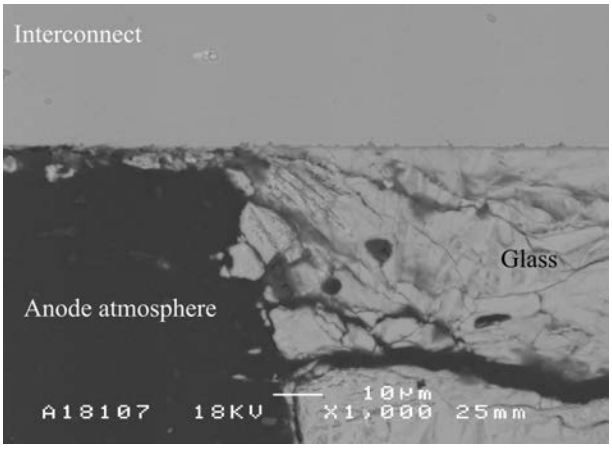

Figure 32. SEM image of the steel/glass interfaces exposed to an anode atmosphere.

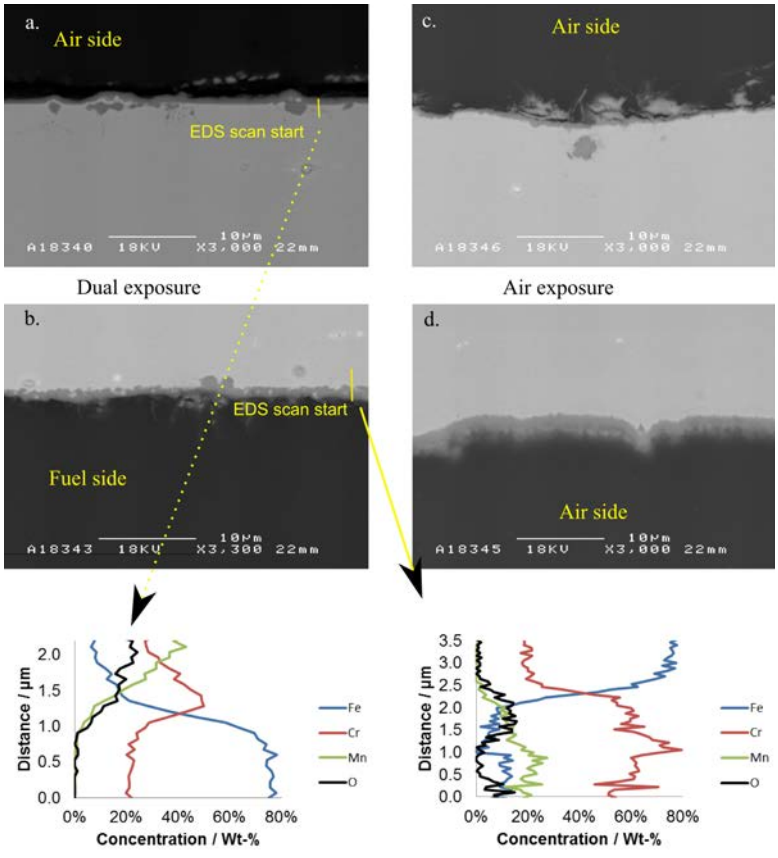

Figure 33. SEM images showing interconnects exposed to a dual atmosphere (left) and an air atmosphere (right).

6. Summary and conclusions

The aim of this thesis was to achieve a performance increase and cost reductions in SOFC stack technology. This goal was pursued by analysis and development of in-stack materials and their behaviour. The SOFC stack creates a challenging environment in which materials are subjected to high temperatures in a dual atmosphere. Therefore, a thorough understanding of the materials is needed to achieve the lifetime and performance increases to which the SOFC research community is committed.

This thesis contributes to the field first by drawing attention to the importance of the mechanical properties of sealing materials and their relation to stack sealing and electrical contact. The mechanical properties of several materials were analysed between room temperature and 700 °C. It is clear that the properties of SOFC sealing materials depend on temperature and their properties need to be evaluated over the given stress and temperature range before using them in-stack. The literature is very short on relevant data on the mechanical properties of these materials. Therefore, the data and guidelines set forth in this work contribute to the field.

To realise cost reductions in SOFC stack technology, it is tempting to reduce stack material usage. Therefore, aiming to lower the necessary compressive stress on the stack is needed to allow for less bulky components to be used. In this thesis, a hybrid sealing solution consisting of compressible core material and glass-based coating was developed. The coating effectively decreased the interfacial leakages and allowed for the material to be used at low compressive stress, down to 0.1 MPa, with leak rates as low as around 0.3 ml (m min)$^{-1}$ using 50/50 H_2/N_2. This is a reduction of about 60…90% compared to the uncoated core material. For example, Chou et al. have measured leak rates of the order of 0.5 ml (m min)$^{-1}$ using mica papers with glass interlayers at compressive stresses of 0.1 MPa [65]. The tests were carried out with 2.64% H_2 in humidified Ar, which, according to the results presented in this work, significantly reduces the observed leak rate compared to 50/50 H_2/N_2. Although different conditions make direct comparison difficult, it is clear that the results presented in this thesis compare favourably with the state-of-the-art SOFC sealing materials. The intellectual property

rights of the hybrid sealing solution presented in this thesis have been transferred to Flexitallic Ltd, which has further developed this technology and issued a patent application on it [72]. In October 2014, they launched a product called Thermiculite 866LS based on this work.

Understanding corrosion phenomena in SOFC stacks is crucial in increasing their lifetime. Compatibility of the developed hybrid seals with the adjacent stack components was analysed. Post-mortem analyses of the stack in which these seals were used showed no signs of seal-induced corrosion. To further increase the lifetime of stacks, a $MnCo_{1.8}Fe_{0.2}O_4$-based protective coating was developed. The coating showed very good stability over 6000 h of in-stack testing. The amount of chromium deposited on the cathode decreased significantly with the coating, compared to the non-coated stack. This development work forms a very good starting point in achieving stack lifetimes of over 10 000 h.

In total, it can be concluded that the targets set for this research work were well met. The materials and methods developed in this work help to realise stacks with lower leak rates and ohmic losses, resulting in higher electrical efficiency. This, together with increased stack lifetime, helps in bringing the price per produced energy unit down.

In the future, understanding of the mechanical properties of SOFC stack sealing materials should be further enhanced. With the methodology presented here, tests should be carried out to find out long-term properties, such as creep and stress retention of the materials. Thermal cycling tests using the hybrid seals should be carried out to find out the effects of coating parameters such as coating thickness and porosity on the seals resistance to thermal cycling. Stack tests or ex-situ tests in realistic conditions with durations of several thousands of hours should also be carried out to further study possible long-term material interactions between interconnects, seals, the coating, and the SOFC cell.

References

[1] W. Schönbein, "Prof. Schönbein's Discussion of M. Fechner's Views of the Theory of Galvanism, with reference, particularly, to a Circuit including Two Electrolytes, and to the relations of Inactive Iron", *London and Edinburgh Philosophical Magazine and Journal of Science*, vol. 10, pp. 161-171, 1938.

[2] K. Kordesch, "25 Years of Fuel Cell Development (1951-1976)", *Journal of the Electrochemical Society*, vol. 125, pp. 77C-88C, Mar. 1978.

[3] B. Pollet, I. Staffell, and J. Shang, "Current status of hybrid, battery and fuel cell electric vehicles: From electrochemistry to market prospects", *Electrichimica Acta*, vol. 84, pp. 235-249, 2012.

[4] FuelCellToday, "The Fuel Cell Industry Review 2013", 2013.

[5] I. Staffell and R. Green, "The cost of domestic fuel cell micro-CHP systems", *International Journal of Hydrogen Energy*, vol. 38, no. 2, pp. 1088-1102, 2013.

[6] K. Krulla et al., "Assessment of the Distributed Generation Market Potential for Solid Oxide Fuel Cells", U.S. Department of Energy, DOE/NETL- 342/093013 2013.

[7] D. Brengel, "Solid State Energy Conversion Alliance (SECA) SOFC Program Review", 2010.

[8] B. James, A. Spisak, and W. Colella, "Manufacturing Cost Analysis of Stationary Fuel Cell Systems", Strategic analysis Inc, 2012.

[9] W. Schafbauer, N. Menzler, and H. Buchkremer, "Tape Casting of Anode Supports for Solid Oxide Fuel Cells at Forschungszentrum Jülich", *International Journal of Applied Ceramic Technology*, vol. 11, no. 1, pp. 125-135, 2014.

[10] Elcogen. (2014, Dec.) Elcogen. [Online]. http://www.elcogen.com/en/sofc-single-cells/technical-data

[11] S. Angeli, G. Monteleone, A. Giaconia, and A. Lemonidou, "State-of-the-art catalysts for CH_4 steam reforming at low temperature", *International Journal of Hydrogen Energy*, vol. 39, pp. 1979-1997, 2014.

[12] SOFCMAN Energy Technology. (2015, Jan.) SOFCMAN Energy Technology. [Online]. http://www.sofc.com.cn

[13] (2014, Dec.) Kerafol. [Online]. http://www.kerafol.com/en/sofc/components-for-fuel-cell-technology/electrolyte-supported-cells-esc.html

[14] B. Borglum, "Solid Oxide Fuel Cell Development at Versa Power Systems" in *2012 Fuel Cell Seminar*, Nov. 2012. [Online]. http://www.fuelcellseminar.com/media/51287/sta42-3.pdf

[15] N. Menzler, F. Tietz, S. Uhlenbruck, H. Buchkremer, and D. Stöver, "Materials and manufacturing technologies for solid oxide fuel cells", *Journal of Material Science*, no. 45, pp. 3109-3135, 2010.

[16] "Fuel Cell Handbook," U.S. Department of Energy, Office of Fossil Energy, National Energy Technology Laboratory, Morgantown, 2004. [Online]. http://www.netl.doe.gov/File%20Library/research/coal/energy%20systems/fuel%20cells/FC Handbook7.pdf

[17] M. Rautanen, O. Himanen, J. Kiviaho, and J. Pennanen, "Method and arrangement for feeding reactants into a fuel cell stack and an electrolyzer stack", Application WO 2014068168 A1, Oct. 31, 2012.

[18] L. Blum et al., "Recent results in Jülich solid oxide fuel cell technology development", *Journal of Power Sources*, no. 241, pp. 477-485, 2013.

[19] B. Borglum, E. Tang, and M. Pastula, "The Status of SOFC Development at Versa Power Systems", *ECS Transactions*, vol. 25, no. 2, pp. 65-70, 2009.

[20] J. Fergus, "Lanthanum chromite-based materials for solid oxide fuel cell interconnects", *Solid State Ionics*, vol. 171, no. 1-2, pp. 1-15, 2004.

[21] T. Armstrong, J. Stevenson, L. Pederson, and P. Raney, "Dimensional Instability of Doped Lanthanum Chromite", *Journal of the Electrochemical Society*, vol. 143, no. 9, pp. 2919-2925, 1996.

[22] Z. Yang, K. Weil, D. Paxton, and J. Stevenson, "Selection and Evaluation of Heat-Resistant Alloys for SOFC Interconnect Applications", *Journal of The Electrochemical Society*, vol. 150, no. 9, pp. A1188-A1201, 2003.

[23] ThyssenKrupp. Crofer 22 H material datasheet, June 2008. [Online]. http://www.fcdic.com/ja/member/data/Crofer22H.pdf

[24] Outokumpu, "AISI 441 Datasheet," *2009*.

[25] Hitachi Metals America. (2014, Dec.) Fuel Cell Interconnector. [Online]. http://www.hitachimetals.com/product/specialtysteel/fuelcellseparator/

[26] M. Schuisky, "Pre-coated 441 strip steel for SOFC interconnects" in *Fuel Cell Seminar*, Orlando, 2011.

[27] Allegheny Technologies Incorporated. (2015, Jan.) E-Brite technical datasheet. [Online]. https://www.atimetals.com/Documents/ati_e-brite_tds_en_v1.pdf

[28] Plansee. (2014, Dec.) CFY: Chromium alloy for SOFC interconnects. [Online]. http://www.plansee.com/en/CFY-1484.htm

[29] Z. Yang, J. Stevenson, D. Paxton, P. Singh, and K. Weil, "Materials Properties Database for Selection of High-Temperature Alloys and Concepts of Alloy Design for SOFC Applications", Pacific Northwest National Laboratory, 2002. [Online]. http://www.pnl.gov/main/publications/external/technical_reports/PNNL-14116.pdf

[30] P. Huczkowski et al., "Oxidation limited life times of chromia forming ferritic steels", *Materials and Corrosion*, vol. 55, no. 11, pp. 825-830, 2004.

[31] J. Froitzheim, H. Ravash, E. Larsson, L. Johansson, and J. Svensson, "Investigation of Chromium Volatilization from FeCr Interconnects by a Denuder Technique", *Journal of The Electrochemical Society*, vol. 157, pp. B1295-B1300, 2010.

[32] E. Opila et al., "Theoretical and Experimental Investigation of the Thermochemistry of $CrO_2(OH)_2(g)$", *Journal of Physical Chemistry A*, vol. 111, pp. 1971-1980, 2007.

[33] O. Thomann, M. Pihlatie, J. Schuler, O. Himanen, and J. Kiviaho, "Method for Measuring Chromium Evaporation from SOFC Balance-of-Plant Components", *ECS Transactions*, vol. 35, pp. 2609-2616, 2011.

[34] J. Fergus, "Effect of cathode and electrolyte transport properties on chromium poisoning in solid oxide fuel cells", *International Journal of Hydrogen Energy*, vol. 32, pp. 3664-3671, 2007.

[35] A. Balland, P. Gannon, M. Deibert, S. Chevalier, G. Caboche, and S. Fontana, "Investigation of La_2O_3 and/or $(Co,Mn)_3O_4$ deposits on Crofer22APU for the SOFC interconnect application", *Surface Coating Technology*, vol. 203, no. 20-21, pp. 3291-3296, 2009.

[36] C. Chu, J. Wang, and S. Lee, "Effects of $La_{0.67}Sr_{0.33}MnO_3$ protective coating on SOFC interconnect by plasma-sputtering", *International Journal of Hydrogen Energy*, vol. 33, no. 10, pp. 2536-2546, 2008.

[37] Z. Yang, G. Xia, G. Maupin and J. Stevenson, "Evaluation of Perovskite Overlay Coatings on Ferritic Stainless Steels for SOFC Interconnect Applications", *Journal of The Electrochemical Society*, vol. 153, pp. A1852-A1858, 2006.

[38] O. Thomann et al., "Development and application of HVOF sprayed protective coatings for SOFC interconnects", *Journal of Thermal Spray Technology,* vol. 22, no. 5, pp. 631-639, 2013.

[39] F. Tietz, D. Sebold, H. Buchkremer, A. Ringuede, M. Cassir, A. Laresgoiti, I. Villarreal and X. Montero, "$MnCo_{1.9}Fe_{0.1}O_4$ spinel protection layer on commercial ferritic steels for interconnect applications in solid oxide fuel cells", *Journal of Power Sources*, vol. 184, no. 1, pp. 172-179, 2008.

[40] D. Lim, D. Lim, J. Oh, and I. Lyo, "Influence of Post Treatments on the Contact Resistance of Plasma-Sprayed $La_{0.8}Sr_{0.2}MnO_3$ Coating on SOFC Metallic Interconnector", *Surface Coating Technology*, vol. 200, no. 5-6, pp. 1248-1251, 2005.

[41] H. Zhai, W. Guan, Z. Li, C. Xu, and W. Wang, "Research on Performance of LSM Coating on Interconnect Materials for SOFCs", *Journal of the Korean Ceramic Society*, vol. 45, no. 12, pp. 777-781, 2008.

[42] M. Garcia-Vargas, M. Zahid, F. Tietz, and A. Aslanides, "Use of SOFC Metallic Interconnect Coated with Spinel Protective Layers Using the APS Technology", *ECS Transactions*, vol. 7, p. 2399, 2007.

[43] S. Fontana et al., "Metallic interconnects for SOFC: Characterisation of corrosion resistance and conductivity evaluation at operating temperature of differently coated alloys", *Journal of Power Sources*, vol. 171, pp. 652-662, 2007.

[44] S. Fontana, S. Chevalier, and G. Caboche, "Performance of reactive element oxide coating during long time exposure" *Materials and Corrosion*, vol. 62, pp. 650-658, 2011.

[45] T. Suntola and J. Antson, "Method for producing compound thin films", U.S. Patent No. 4058430, 1977.

[46] D. Gödeke, J. Besinger, Y. Pflügler, and B. Ruedinger, "New Glass Ceramic Sealants for SOFCs", vol. 25, no. 2, pp. 1483-1490, 2009.

[47] J. Suffner and C. Dobler, "Long Term Behavior of Viscous High-Temperature Sealing Glasses", *ECS Transactions*, vol. 57, pp. 2375-2383, 2013.

[48] VIOX. (2014, Dec.) Glass Options for SOFC Applications. [Online]. http://viox.thomasnet.com/viewitems/electronic-specialty-glass/glass-options-for-sofc-seal-applications-2?

[49] T. Ertugrul, S. Celik, and M. Mat, "Effect of binder burnout on the sealing performance of glass ceramics for solid oxide fuel cells", *Jounal of Power Sources*, no. 242, pp. 775-783, 2013.

[50] A. Shyam et al., "Microstructural evolution in two alkali multicomponent silicate glasses as a result of long-term exposure to solid oxide fuel cell environments", *J Mater Sci*, 2013.

[51] K. Weil, "The state-of-the-art in sealing technology for solid oxide fuel cells", *The Journal of The Minerals, Metals & Materials Society (TMS)*, vol. 58, no. 8, pp. 37-44, 2006.

[52] V. Kumar, A. Arora, O. Pandey, and K. Singh, "Studies on thermal and structural properties of glasses as sealants for solid oxide fuel cells", *International Journal of Hydrogen Energy*, vol. 33, pp. 434-438, 2008.

[53] L. Blum et al., "Investigation of solid oxide fuel cell sealing behaviour under stack relevant conditions at Forschungzentrum Jülich", *Journal of Power Sources*, vol. 196, no. 17, pp. 7175-7181, 2011.

[54] M. Peksen, A. Al-Masri, L. Blum, and D. Stolten, "3D transient thermomechanical behaviour of a full scale SOFC short stack", *International journal of hydrogen energy*, vol. 38, pp. 4099-4107, 2013.

[55] G. Wypych, *Handbook of Fillers – A Definitive User's Guide and Databook*, 2nd ed. Toronto, Canada: ChemTec Publishing, 2000.

[56] P. Ciullo, Ed., *Industrial Minerals and Their Uses – A Handbook and Formulary*. Noyes, Westwood, USA: William Andrew Publishing, 1996.

[57] Feodor Burgmann Dichtungswerke GmbH, *Sealing Technology*, vol. 6, 2000.

[58] Y. Chou, J. Stevenson, and L. Chick, "Ultra-low leak rate of hybrid compressive mica seals for", *Journal of Power Sources*, vol. 112, no. 1, pp. 130-136, 2002.

[59] Y. Chou, J. Stevenson, and L. Chick, "Novel compressive mica seals with metallic interlayers", *Journal of the American Ceramic Society*, vol. 86, no. 6, pp. 1003-1007, 2003.

[60] M. Rautanen, O. Himanen, V. Saarinen, and J. Kiviaho, "Compression Properties and Leakage Tests of Mica-Based Seals for SOFC applications", *Fuel Cells*, pp. 753-759, 2009.

[61] S. Simner and J. Stevenson, "Compressive mica seals for SOFC applications", *Journal of Power Sources*, vol. 102, no. 1-2, pp. 310-316, 2001.

[62] M. Bram et al., "Deformation behavior and leakage tests of alternate sealing materials for SOFC stacks", *Journal of Power Sources*, vol. 138, no. 1-2, pp. 111-119, 2004.

[63] J. Hoyes and S. Bond, "Gaskets for sealing solid oxide fuel cells", *Sealing Technology*, no. 8, pp. 11-14, 2007.

[64] J. Hoyes and M. Rautanen, "SOFC Sealing with Thermiculite 866 and Thermiculite 866 LS", *ECS Transactions*, vol. 57, no. 1, pp. 2365-2374, 2013.

[65] Y. Chou and J. Stevenson, "Long-term ageing and materials degradation of hybrid mica", *Journal of Power Sources*, vol. 191, no. 2, pp. 384-389, 2009.

[66] Y. Chou, J. Stevenson, and P. Singh, "Thermal cycle stability of a novel glass-mica composite", *Journal of Power Sources*, vol. 152, no. 1-2, pp. 168-174, 2005.

[67] M. Rautanen, V. Pulkkinen, J. Tallgren, O. Himanen, and J. Kiviaho, "Effects of the first heat up procedure on mechanical properties of solid oxide fuel cell sealing materials", *Journal of Power Sources*, vol. 284, pp. 511-516, 2015.

[68] V. Haanappel, V. Shemet, I. Vinke and W. Quadakkers, "A novel method to evaluate the suitability of glass sealant–alloy combinations under SOFC stack conditions", *Journal of Power Sources*, vol. 141, no. 1, pp. 102-107, 2005.

[69] M. Mahapatra and K. Lu, "Glass-based seals for solid oxide fuel and electrolyzer cells – A review", *Materials Science and Engineering*, vol. 67, no. 5-6, pp. 65-85, 2010.

[70] *ASTM D445-15 Standard Test Method for Kinematic Viscosity of Transparent and Opaque Liquids (and Calculation of Dynamic Viscosity)*.: ASTM International.

[71] M. Rautanen, O. Thomann, O. Himanen, J. Tallgren, and J. Kiviaho, "Glass coated compressible solid oxide fuel cell seals", *Journal of Power Sources*, vol. 247, pp. 243-248, 2014.

[72] M. Rautanen, J. Hoyes, O. Himanen, and J. Kiviaho, "Gasket for fuel cells", Application PCT/GB2014/050161 WO2014111735 A1, Jan. 21, 2013.

[73] N. Menzler et al., "Studies of Material Interaction After Long-Term Stack Operation", *Fuel Cells*, vol. 07, no. 05, pp. 356-363, 2007.

[74] W. Liu and E. Konysheva, "Conductivity of $SrCrO_4$ and its Influence on Deterioration of Electrochemical Performance of Cathodes in Solid Oxide Fuel Cells", *ECS Transactions*, vol. 59, pp. 327-332, 2014.

[75] N. Shaigan, W. Qu, D. Ivey and W. Chen, "A Review of Recent Progress in Coatings, Surface Modifications and Allou Developments for Solid Oxide Fuel Cell Ferritic Stainless Steel Interconnects", *Journal of Power Sources*, vol. 195, no. 6, pp. 1529-1542, 2010.

[76] Y. Larring and T. Norby, "Spinel and Perovskite Functional Layers Between Plansee Metallic Interconnect (Cr-5 Wt% Fe-1 Wt% Y_2O_3) and Ceramic $(La_{0.8}Sr_{0.15})_{0.91}MnO_3$ Cathode Materials for Solid Oxide Fuel Cells", *Journal of the Electrochemical Society*, vol. 147, no. 9, pp. 3251-3256, 2000.

[77] J. Puranen et al., "The Structure and Properties of Plasma Sprayed Iron Oxide Doped Manganese Cobalt Oxide Spinel Coatins for SOFC Metallic Interconnectors", *Journal of Thermal Spray Technology*, vol. 20, no. 1-2, pp. 154-159, 2011.

[78] J. Lagerbom et al., "$MnCo_2O_4$ Spinel Chromium Barrier Coatings for SOFC Interconnects by HVOF", in *9th Liege Conference on Materials for Advanced Power Engineering*, 2010, pp. 925-932.

Series title and number

VTT Science 97

Title	**Improving sealing, electrical contacts, and corrosion resistance in solid oxide fuel cell stacks**
Author(s)	Markus Rautanen
Abstract	In solid oxide fuel cell systems, the stack is the primary component whose performance and lifetime should be maximized while decreasing the cost. In this thesis, leakages, electrical contact resistance, and corrosion resistance in SOFC stacks were studied and developed. Typically, SOFC stacks are assembled at room temperature, then heated up and conditioned, and then operated at temperatures in the range of 600...900 °C. Therefore, the mechanical properties of seals should be understood from room temperature to operating temperature. Of special interest are the mechanical properties of materials during the first heat up, in which the stack is sealed, reduced, and tested. Mechanical properties of glass and compressible sealing materials were studied with different heat-up procedures. It was noticed that with compressible Thermiculite 866 or CL87 materials, the compressibility is diminished after the first heat up, and therefore it is beneficial to apply compression before heating, to obtain maximum deformation capability of the seal. The progress in manufacturing SOFC cells is leading to an increase in cell area. From the perspective of compressible seals, the increase in cell area presents a challenge: the higher the cell area, the higher the required compressive force for the stack. For this purpose, a hybrid sealing material capable of maintaining leak rates below 1% of the inlet fuel flow below 1 MPa of compressive stress was developed. The material consists of a compressible core of Thermiculite 866, a commercial material consisting of vermiculite and steatite, and a conformable glass-based interlayer. The interlayers seal the mating surfaces, thus diminishing the leakages through the interfaces. Using the coating technique, leak rates were diminished by 60...90% compared to the uncoated seals. Post-mortem analyses of a stack also showed no signs of corrosion caused by the glass-coating. A high operating temperature and exposure to both reducing and oxidizing atmospheres is prone to cause corrosion of materials. One example of these corrosion-related deactivation mechanisms is chromium evaporation from interconnect steel materials. The evaporated chromium is transported in the gas phase to the electrochemically active cell, where it can solidify to chromium oxide, causing loss of performance. These phenomena can be mitigated with chromium barrier coatings on interconnect steels. A $MnCo_{1.8}Fe_{0.2}O_4$ coating deposited by a high-velocity oxygen flame (HVOF) method was prepared and tested both with ex-situ and stack tests. The prepared coating showed good stability and low area-specific resistivity, and was found to hinder chromium transport to the electrochemical cell.
ISBN, ISSN	ISBN 978-951-38-8313-3 (Soft back ed.) ISBN 978-951-38-8314-0 (URL: http://www.vtt.fi/publications/index.jsp) ISSN-L 2242-119X ISSN 2242-119X (Print) ISSN 2242-1203 (Online)
Date	June 2015
Language	English, Finnish abstract
Pages	68 p. + app. 59 p.
Name of the project	
Commissioned by	
Keywords	SOFC, stack, seal, leak, corrosion, contact, chromium
Publisher	VTT Technical Research Centre of Finland Ltd P.O. Box 1000, FI-02044 VTT, Finland, Tel. 020 722 111

Julkaisun sarja ja numero

VTT Science 97

Nimeke	**Kiinteäoksidipolttokennostojen tiivisteiden, sähköisten kontaktien ja korroosiosuojauksen kehittäminen**
Tekijä(t)	Markus Rautanen
Tiivistelmä	Kiinteäoksidipolttokennojärjestelmän tärkein komponentti on kennosto, jonka suorituskyky ja elinikä pyritään maksimoimaan samalla kun kustannukset pyritään minimoimaan. Tässä väitöskirjassa tutkittiin ja kehitettiin kiinteäoksidipolttokennoston tiivisteitä sekä keskityttiin parantamaan kennoston sisäistä sähköistä kontaktia ja korroosiokestävyyttä. Kiinteäoksidipolttokennostojen kokoonpano tapahtuu huoneenlämpötilassa, minkä jälkeen ne lämmitetään ja esikäsitellään tyypillisesti 600...900 °C lämpötila-alueella. Tämän vuoksi tiivistemateriaalien mekaaniset ominaisuudet tulee tuntea koko lämpötila-alueella huoneenlämpötilasta käyttölämpötilaan saakka. Erityisen tarkastelun kohteena ovat mekaaniset ominaisuudet ensimmäisessä lämmityksessä, jonka aikana kennosto tiivistetään, pelkistetään ja testataan. Erilaisten puristus- ja lämmitystapojen vaikutusta tiivisteiden mekaanisiin ominaisuuksiin tutkittiin kokeellisesti. Testattujen kokoonpuristuvien tiivisteiden (Thermiculite 866 & CL87) kokoonpuristuvuuden havaittiin vähentyvän lämmityksen jälkeen. Näin ollen kennoston kannalta optimaalista on suorittaa kennoston ensimmäinen puristus huoneenlämpötilassa. SOFC-kennojen pinta-alan kasvu tuottaa haasteita kokoonpuristuville tiivisteille, koska pinta-alan kasvaessa kennoston puristamiseksi tarvitaan suurempi voima. Työssä kehitettiin hybriditiiviste, jolla voidaan saavuttaa alle 1% vuototaso suhteessa polttoainevirtaukseen pienilläkin, alle 1 MPa, puristuspaineilla. Kehitetty tiivisteratkaisu koostuu kokoonpuristuvasta Thermiculite 866 substraatista, joka pinnoitettiin lasia sisältävällä seoksella. Pinnoitetun tiivisteen vuototasojen mitattiin olevan 60...90% pienemmät suhteessa pinnoittamattomaan tiivisteeseen. Pinnoitteen ja virtauskanavalevyjen tai kennojen välillä ei myöskään havaittu tiivisteistä johtuvaa korroosiota. Kiinteäoksidipolttokennojen korkea käyttölämpötila ja kaksoiskaasukehä aiheuttavat helposti materiaalien välistä korroosiota. Ehkä merkittävin korroosioilmiö on kromin höyrystyminen virtauskanavalevyjen teräksistä ja kulkeutuminen sähkökemiallisesti aktiivisiin kennoihin, joihin kiteytyessään se vähentää suorituskykyä. Tämän ilmiön pienentämiseksi työssä valmistettiin $MnCo_{1.8}Fe_{0.2}O_4$-pinnoitettuja virtauskanavalevyjä ja testattiin niitä sekä ex-situ-kokeilla että kennostossa. Pinnoitteen havaittiin ehkäisevän kromin höyrystymistä ja siten parantavan kennoston elinikää.
ISBN, ISSN	ISBN 978-951-38-8313-3 (nid.) ISBN 978-951-38-8314-0 (URL: http://www.vtt.fi/publications/index.jsp) ISSN-L 2242-119X ISSN 2242-119X (Painettu) ISSN 2242-1203 (Verkkojulkaisu)
Julkaisuaika	Kesäkuu 2015
Kieli	Englanti, suomenkielinen tiivistelmä
Sivumäärä	68 s. + liitt. 59 s.
Projektin nimi	
Rahoittajat	
Avainsanat	SOFC, stack, seal, leak, corrosion, contact, chromium
Julkaisija	Teknologian tutkimuskeskus VTT Oy PL 1000, 02044 VTT, puh. 020 722 111

Improving sealing, electrical contacts, and corrosion resistance in solid oxide fuel cell stacks

Solid oxide fuel cells are high temperature electrochemical devices for direct conversion of fuel and oxidant to electricity and heat. The high temperature and dual atmosphere creates challenges for the materials in solid oxide fuel cell stacks. In this thesis SOFC stack materials were studied and developed.

SOFC stacks are assembled at room temperature, then heated up, conditioned and operated at 600...900 °C. Therefore, the mechanical properties of seals should be understood from room temperature to operating temperature. Mechanical properties of SOFC sealing materials were studied with different heat-up procedures.

Increasing cell footprint presents a challenge for the sealing: the higher the cell area, the higher the required compressive force for the stack. To diminish the required compressive force, a hybrid sealing material consisting of a compressible core and a conformable glass-based interlayer was developed. This hybrid sealing material decreased leak rates by 60...90% compared to the conventional compressible seals.

High operating temperature and exposure to both reducing and oxidizing atmospheres is prone to cause corrosion of materials. One example of these corrosion-mechanisms is chromium evaporation from interconnect steel materials. The evaporated chromium is transported in the gas phase to the electrochemically active cell, where it can solidify to chromium oxide, causing loss of performance. A chromium barrier coating based on $MnCo_{1.8}Fe_{0.2}O_4$ was developed and deposited by a high-velocity oxygen flame method on the interconnect steel. The coating showed good stability and low area-specific resistivity, and effectively hindered chromium transport to the electrochemical cell.

ISBN 978-951-38-8313-3 (Soft back ed.)
ISBN 978-951-38-8314-0 (URL: http://www.vtt.fi/publications/index.jsp)
ISSN-L 2242-119X
ISSN 2242-119X (Print)
ISSN 2242-1203 (Online)